ADAPTIVE MESH FOR ELASTICITY UNDER TRACTION BOUNDARY CONDITION USING HIGHER ORDER FEM

MAHARAVO RANDRIANARIVONY

Abstract. Our emphasis is on the use of a-posteriori error estimators to control adaptive refinements for problems obeying the equation of elasticity. The problems are subject to both Dirichlet and Neumann boundary conditions. Using adaptivity together with higher polynomial degrees considerably reduces the degree of freedom to achieve a high precision. We study the agreement of the a-posteriori error estimates and the exact precisions for every polynomial degree. The advantage of using higher polynomial degrees is shown by using some benchmarks including a punctual accumulation, an internal layer and a re-entrant corner. We report briefly on some results in the 3D case including a parallel tetrahedral mesh refinement and the von Mises stress on a concrete CAD model.

1. Introduction

Our motivation for using higher polynomial degrees [7, 9, 17, 18, 27, 28] to treat the elasticity problem [1, 13, 3] is that it efficiently overcomes the locking phenomenon [6, 31]. In some cases, the piecewise linear setting could fail to converge when increasing the degree of freedom. We concentrate in this document on completely homogeneous and incompressible elastic materials which obey the Navier-Lamé equation constrained to Dirichlet and Neumann boundary conditions. The latter is physically interpreted as traction in practical elastostatic simulations [1]. For the sake of presentation simplicity, the approach is mainly described in 2D but it can be easily extended in the 3D case. Since the exact solution is not known for real applications, an error estimator is needed [12, 22, 26, 29, 30, 32, 14]. We use an error estimator which is efficient and reliable but the bounding constants could depend on the material properties. A further function of the error estimator is to identify the regions within the simulation domain where the precision is unsatisfactory. Mesh refinements [4, 5, 8] are therefore applied at those regions to improve the local precision. We treat polynomial inverse estimates together with their applications to higher order FEM by computing elastostatic simulation. The estimates describe inequalities of polynomials of given degree in term of weighted Sobolev norms. In [17, 18], some such inverse estimates are already documented but they use another type of weights. In effect, their weight function is expressed as the distance of a point from the boundary of a triangle. In contrast, we

consider weight functions which are expressed in barycentric coordinates. That makes it computationally efficient to evaluate. Polynomial inverse estimates are not only important for theoretical purpose. They do also appear in practical application of a-posteriori estimators. In fact, the estimators have to be evaluated in every element of the entire mesh. Thus, in order to compute the APEE (a-posteriori error estimator) in practice, the weight functions need to be evaluated a large number of times. It is therefore important to have a function which is not intensive to evaluate. Verfürth has compiled a comprehensive study [29] about APEE for which he mainly treats piecewise linear FEM. Many different a-posteriori error estimators have been proposed for the Stokes problem [30, 2, 22, 25]. An interesting APEE for two and three dimensions as well as an anisotropic adaptive mesh refinement are also detailed in [26]. Our approach is inspired from the works in [17, 9] which both treat mainly the Poisson problem for purely homogeneous Dirichlet boundary condition. For the Spectral Element Method, we find in [9] an APEE for the hp-case which has been generalized in [17] to treat hp-FEM [18] for the Poisson problem where corner singularities are allowed. We have presented in [22] an APEE based on hierarchical space enrichment on anisotropic FEM which is combined with adaptive refinements. As far as mesoscale molecular elasticity is concerned, a simulation for chemical quantum computation using FEM is documented in [13] where we have used nanotubes immersed in polymer matrices. The exposition of this document is structured as follows. The next section introduces the higher order FEM setting, several notations and some preliminary notions on elasticity. The following section is occupied by the description of the error estimator. That involves multiple local estimators: interior, at faces separating two elements, at faces situated at the Neumann boundary. The investigation of its efficiency and reliability is also analyzed. In the last section, we highlight the advantage of adaptive refinements over uniform ones. The adaptivities are illustrated by the refinement histories. To gain more confidence, we vary the parameters of the estimator and the problem coefficients because the constants about the estimates are not explicitly known theoretically. We consider several benchmarks: a punctual accumulation, an internal layer and a re-entrant corner. We show the advantage of the higher order setting over the piecewise linear case. In fact, for a comparable size of degree of freedom, one achieves better accuracies by using higher polynomial degrees for locally smooth solutions. In addition, we investigate the alignment between the estimates and the exact accuracies for several polynomial degrees. The von Mises stress is computed on a realistic CAD model [1, 19, 21, 23, 24] where the mesh distribution after adaptive refinements tends to be dense at positions in which the von Mises stress is large.

2. Higher order FEM discretizations

When an elastic model $\mathbf{\Omega}$ bounded by $\mathbf{\Gamma} = \partial\mathbf{\Omega}$ is under constraints of a body force and prescribed boundary conditions, it has the displacement function $\mathbf{U} : \mathbf{\Omega} \longrightarrow \mathbb{R}^2$ where $\mathbf{U} = (U_1, U_2)^{\mathrm{T}}$. We suppose $\mathbf{\Omega}$ admits the elastic properties which are specified by the Lamé coefficients (λ, μ) whose relation with the Young's modulus E and the Poisson ratio ν is $\lambda = E\nu/[(1+\nu)(1-2\nu)]$, $\mu = E/[2(1+\nu)]$. Throughout, vector values are supposed to be column vectors. Thus, the scalar product of $\mathbf{a}$ and $\mathbf{b}$ is denoted by $\mathbf{a}^{\mathrm{T}}\mathbf{b}$ while the norm is denoted by $|\mathbf{a}| = \sqrt{\mathbf{a}^{\mathrm{T}}\mathbf{a}}$. By using isotropic homogeneous materials, the strain and stress tensors are defined as

$$\boldsymbol{\varepsilon}(\mathbf{U}) = \big[\varepsilon_{ij}(\mathbf{U})\big]_{i,j} = 0.5\big[(\nabla\mathbf{U}) + (\nabla\mathbf{U})^{\mathrm{T}}\big] \tag{2.1}$$

$$\boldsymbol{\sigma}(\mathbf{U}) = \big[\sigma_{ij}(\mathbf{U})\big]_{i,j} = 2\mu\boldsymbol{\varepsilon}\big(\mathbf{U}\big) + \lambda\,\mathrm{Trace}\big[\boldsymbol{\varepsilon}\big(\mathbf{U}\big)\big]\mathbf{I}_2 \tag{2.2}$$

where $\nabla\mathbf{U}$ denotes the matrix having $\partial_i U_j$ as coefficients. We assume that the boundary $\mathbf{\Gamma} = \partial\mathbf{\Omega}$ is decomposed into Dirichlet and Neumann boundaries as $\mathbf{\Gamma} = \mathbf{\Gamma}_D \cup \mathbf{\Gamma}_N$ such that $\mathbf{\Gamma}_D$ and $\mathbf{\Gamma}_N$ are not overlapping and $\mathbf{\Gamma}_D \neq \emptyset$. We consider the Navier-Lamé equation with homogeneous Dirichlet and Neumann boundary conditions:

$$\left\{\begin{array}{lcll} -\mathrm{div}\big[\boldsymbol{\sigma}\big(\mathbf{U}(\mathbf{x})\big)\big] &=& \mathbf{f}(\mathbf{x}) & \text{for} \quad \mathbf{x} \in \mathbf{\Omega} \\ \mathbf{U}(\mathbf{x}) &=& \mathbf{0} & \text{for} \quad \mathbf{x} \in \mathbf{\Gamma}_D \\ \boldsymbol{\sigma}\big(\mathbf{U}(\mathbf{x})\big)\mathbf{n}(\mathbf{x}) &=& \mathbf{g}(\mathbf{x}) & \text{for} \quad \mathbf{x} \in \mathbf{\Gamma}_N \end{array}\right. \tag{2.3}$$

in which $\mathbf{n}(\mathbf{x})$ is the unit normal vector point outward at $\mathbf{x} \in \mathbf{\Gamma}_N$ while $\mathbf{f} = [f_1, f_2]^{\mathrm{T}}$ represents a given body force function and $\mathbf{g} = [g_1, g_2]^{\mathrm{T}}$ is given on the Neumann boundary. The space of square integrable functions and the Sobolev space of order k in $\mathbf{\Omega}$ are respectively denoted by $\mathbb{L}^2(\mathbf{\Omega})$ and $\mathbb{H}^k(\mathbf{\Omega})$ which are endowed with the norms $\big\|\bullet\big\|_{\mathbb{L}^2(\mathbf{\Omega})}$ and $\big\|\bullet\big\|_{\mathbb{H}^k(\mathbf{\Omega})}$. Introduce

$$\mathbb{H}^1_{\mathbf{\Gamma}_D}(\mathbf{\Omega}) := \big\{f \in \mathbb{H}^1(\mathbf{\Omega}) : \quad f = 0 \quad \text{in} \quad \mathbf{\Gamma}_D\big\}. \tag{2.4}$$

The vector/matrix valued Sobolev spaces are componentwise of the scalar valued Sobolev spaces. The above Navier-Lamé equation corresponds to the partial differential operator $-\mu\Delta\mathbf{U} - (\mu+\lambda)\mathbf{grad}\,(\mathrm{div}\,\mathbf{U})$ which is associated to the bilinear form

$$\mathcal{A}(\mathbf{U},\mathbf{V}) := \int_{\mathbf{\Omega}} \sum_{i,j} 2\mu\varepsilon_{ij}\big(\mathbf{U}(\mathbf{x})\big)\varepsilon_{ij}\big(\mathbf{V}(\mathbf{x})\big) + \lambda\mathrm{div}\big(\mathbf{U}(\mathbf{x})\big)\mathrm{div}\big(\mathbf{V}(\mathbf{x})\big)d\mathbf{x} \tag{2.5}$$

$$= \int_{\mathbf{\Omega}} \boldsymbol{\varepsilon}(\mathbf{U}(\mathbf{x})) : \boldsymbol{\sigma}(\mathbf{V}(\mathbf{x}))\, d\mathbf{x} \tag{2.6}$$

where $A : B := \sum_{i,j} A_{ij}B_{ij}$. The resulting energy norm $\|\!|\!| \bullet |\!|\!|_E := \mathcal{A}(\bullet,\bullet)^{1/2}$ is

$$\big|\!\big|\!\big|\mathbf{U}\big|\!\big|\!\big|_E^2 = 2\mu\big\|\boldsymbol{\varepsilon}(\mathbf{U})\big\|^2_{[L_2(\mathbf{\Omega})]^{2\times 2}} + \lambda\big\|\mathrm{div}(\mathbf{U})\big\|^2_{[L_2(\mathbf{\Omega})]^2}. \tag{2.7}$$

We assume the following equivalence

$$C_1\|\mathbf{U}\|_{[\mathbb{H}^1(\mathbf{\Omega})]^2} \leq \|\!|\mathbf{U}|\!\|_E \leq C_2\|\mathbf{U}\|_{[\mathbb{H}^1(\mathbf{\Omega})]^2} \tag{2.8}$$

where C_1, C_2 may depend on (λ, μ). The conormal derivative of a function $\mathbf{u}$ is given componentwise [16] by

$$[\boldsymbol{\gamma}_1\mathbf{u}]_i(\mathbf{x}) = \sum_{j=1}^{2} \nu_j(\mathbf{x})\sigma_{ij}[\mathbf{u}(\mathbf{x})] \tag{2.9}$$

In practical applications, the conormal derivative coincides with the traction. The Galerkin variational formulation is

$$\int_{\mathbf{\Omega}} \boldsymbol{\varepsilon}[\mathbf{U}(\mathbf{x})] : \boldsymbol{\sigma}[\mathbf{V}(\mathbf{x})]d\mathbf{x} = \int_{\mathbf{\Omega}} [\mathbf{f}(\mathbf{x})]^{\mathrm{T}}\mathbf{V}(\mathbf{x})d\mathbf{x} + \int_{\mathbf{\Gamma}_N} [\mathbf{g}(\mathbf{x})]^{\mathrm{T}}\mathbf{V}(\mathbf{x})d_{\mathbf{\Gamma}}\mathbf{x} \tag{2.10}$$

for all $\mathbf{V} \in \left[\mathbb{H}^1_{\mathbf{\Gamma}_N}(\mathbf{\Omega})\right]^2$. For the FEM treatment of the above problem, we use a mesh $\mathbb{M}_h(\mathbf{\Omega})$ composed of triangles admitting the next two properties. First, the intersection of two different elements $T_i, T_j \in \mathbb{M}_h(\mathbf{\Omega})$ is either empty or a common node or a complete edge. Second, we have the coverings $\mathbf{\Omega} = \bigcup_{T\in\mathbb{M}_h(\mathbf{\Omega})} T$. For a triangle $T \in \mathbb{M}_h(\mathbf{\Omega})$, we denote by $h(T)$ and $\rho(T)$ its diameter and supremum of the diameters of all balls contained in T while its aspect ratio is define as $\sigma(T) := h(T)/\rho(T)$. We assume quasi-uniformity in the sense that there exists a constant $\sigma_0 > 0$ such that

$$\sigma(T) \leq \sigma_0 < \infty \qquad \text{for all} \qquad T \in \mathbb{M}_h(\mathbf{\Omega}). \tag{2.11}$$

Define

$$\begin{aligned} \mathcal{N}_0(T) &:= \text{ set of elements of } \mathbb{M}_h(\mathbf{\Omega}) \text{ sharing a vertex with } T, \\ \mathcal{N}_i(T) &:= \text{ set of elements of } \mathbb{M}_h(\mathbf{\Omega}) \text{ sharing a vertex with } T' \in \mathcal{N}_{i-1}(T). \end{aligned}$$

We use $\mathcal{N}(T)$ to denote $\mathcal{N}_i(T)$ for sufficiently large i. We define the following subsets of edges

$$\begin{aligned} \mathbb{E}_h(\mathbf{\Gamma}_N) &:= \text{ set of edges of } \mathbb{M}_h(\mathbf{\Omega}) \text{ on the Neumann boundary } \mathbf{\Gamma}_N, \\ \mathbb{E}_h(\mathbf{\Omega}) &:= \text{ set of edges of } \mathbb{M}_h(\mathbf{\Omega}) \text{ which are not included in } \mathbf{\Gamma} = \mathbf{\Gamma}_D \cup \mathbf{\Gamma}_N. \end{aligned}$$

Note that an edge of $\mathbb{E}_h(\mathbf{\Omega})$ may have an endpoint in $\mathbf{\Gamma}$. For an edge e, we denote by $h(e)$ and $\mathcal{N}(e)$ the length of e and the set of elements of $\mathbb{M}_h$ having e as a side. We denote by $\mathbf{n}(e)$ the unit normal vector orthogonal to e. The direction of $\mathbf{n}(e)$ is outward $\mathbf{\Gamma}_N$ if the edge $e \in \mathbb{E}_h(\mathbf{\Gamma}_N)$ whereas, it is pointed in an arbitrary but fixed orientation for $e \in \mathbb{E}_h(\mathbf{\Omega})$.

For a higher order FEM setting, the finite dimensional subspace of $\left[\mathbb{H}^1_{\mathbf{\Gamma}_N}(\mathbf{\Omega})\right]^2$ is

$$\mathcal{S}_h := \left\{ \mathbf{W} \in \left[\mathcal{C}^0(\mathbf{\Omega}) \cap \mathbb{H}^1_{\mathbf{\Gamma}_D}(\mathbf{\Omega})\right]^2 \;\middle|\; \begin{array}{l} \mathbf{W} = (W_1, W_2), \\ W_i \in \mathcal{P}_p(T) \quad \forall\, T \in \mathbb{M}_h(\mathbf{\Omega}),\, \forall\, i = 1, 2 \end{array} \right\} \tag{2.12}$$

where $\mathcal{C}^0$ is the space of continuous functions, $\mathcal{P}_p(T)$ denotes the space of polynomials in T spanned by the monomials $x_1^i x_2^j$ where $0 \leq i+j \leq p$. The approximated variational formulation consists in searching for $\mathbf{U}_h \in \mathcal{S}_h$ such that for all $\mathbf{V}_h \in \mathcal{S}_h$

$$\int_{\mathbf{\Omega}} \boldsymbol{\varepsilon}[\mathbf{U}_h(\mathbf{x})] : \boldsymbol{\sigma}[\mathbf{V}_h(\mathbf{x})] d\mathbf{x} = \int_{\mathbf{\Omega}} [\mathbf{f}(\mathbf{x})]^{\mathrm{T}} \mathbf{V}_h(\mathbf{x}) d\mathbf{x} + \int_{\mathbf{\Gamma}_N} [\mathbf{g}(\mathbf{x})]^{\mathrm{T}} \mathbf{V}_h(\mathbf{x}) d_{\mathbf{\Gamma}}\mathbf{x}. \tag{2.13}$$

3. Higher order a-posteriori error estimator

For any element $T \in \mathbb{M}_h(\mathbf{\Omega})$, the affine invertible mapping from the unit reference

$$\widehat{T} := \Big\{ \mathbf{x} = (x, y) \in \mathbf{R}^2 : 0 \leq x \leq 1,\ 0 \leq y \leq 1,\ 0 \leq x + y \leq 1 \Big\} \tag{3.14}$$

onto T is denoted by $F_T : \widehat{T} :\longrightarrow T$ in which $F_T\mathbf{x} = B\mathbf{x} + b$ that fulfills

$$\det(B) = \mathcal{O}(h^2(T)), \quad \det(B^{-1}) = \mathcal{O}(h^{-2}(T)) \tag{3.15}$$

due to the shape regularity (2.11). For a triangle $T = \{(x_0, y_0), (x_1, y_1), (x_2, y_2)\}$, we denote the barycentric coordinates $\lambda_{i,T}(x, y)$ for $i = 0, 1, 2$. For a triangle T, the barycentric weight function is expressed for $\mathbf{x} \in T$ as

$$\omega_T(\mathbf{x}) = \lambda_{0,T}(\mathbf{x})\lambda_{1,T}(\mathbf{x})\lambda_{2,T}(\mathbf{x}) \tag{3.16}$$

which takes zero values at the boundary of the triangle T. It is a generalization of the unidimensional Gegebauer weight (also known as Jacobi weight) which is defined on the unit interval $[0, 1]$ as

$$\omega_{[0,1]}(t) := t(1 - t) \qquad \forall\, t \in [0, 1]. \tag{3.17}$$

We suppose that we dispose of the approximated solution $\mathbf{U}_h$ and our purpose is to estimate the error $\|\mathbf{U} - \mathbf{U}_h\|_{[\mathbb{H}^1(\mathbf{\Omega})]^2}$. For an element $T \in \mathbb{M}_h(\mathbf{\Omega})$, the estimator is defined as

$$\eta_{\alpha,T}^{\mathbf{elem}} := \frac{h(T)}{p} \Big\| \big[\mathbf{f}_T + \mu\Delta\mathbf{U}_h + (\mu + \lambda)\mathbf{grad}(\operatorname{div} \mathbf{U}_h)\big]\omega_T^{\alpha/2} \Big\|_{\left[\mathbb{L}^2(T)\right]^2} \tag{3.18}$$

where $\mathbf{f}_T$ designates the $\mathbb{L}_2(T)$-projection of the body force $\mathbf{f}$ onto the element T. For an edge $e \in \mathbb{E}_h(\mathbf{\Gamma}_N)$, define

$$\eta_{\alpha,e}^{\mathbf{Neum}} := \sqrt{\frac{h(e)}{2p}} \Big\| \big[\mathbf{g}_e - \boldsymbol{\sigma}(\mathbf{U}_h)_{|_{T_e}} \mathbf{n}(e)\big]\omega_e^{\alpha/2} \Big\|_{\left[\mathbb{L}^2(e)\right]^2} \tag{3.19}$$

where T_e is the element incident upon e and $\mathbf{g}_e$ is the $\mathbb{L}_2(e)$-projection of $\mathbf{g}$ onto the edge e while ω_e is the transformation of (3.17) on the edge e. The estimator for an interior edge $e \in \mathbb{E}_h(\mathbf{\Omega})$ having a normal vector $\mathbf{n}(e)$ is defined as

$$\eta_{\alpha,e}^{\mathbf{inter}} := \sqrt{\frac{h(e)}{2p}} \Big\| \big[\boldsymbol{\sigma}(\mathbf{U}_h)_{|_{T_{(1,e)}}} \mathbf{n}(e) - \boldsymbol{\sigma}(\mathbf{U}_h)_{|_{T_{(2,e)}}} \mathbf{n}(e)\big]\omega_e^{\alpha/2} \Big\|_{\left[\mathbb{L}^2(e)\right]^2} \tag{3.20}$$

where $T_{(1,e)}$ and $T_{(2,e)}$ are the elements incident upon the edge e. Since one needs computable local estimators for an element-by-element computation, an interior element $T \in \mathbb{M}_h(\mathbf{\Omega})$ is introduced

$$\eta_{\alpha,T}^{\mathbf{loc}} := \left[(\eta_{\alpha,T}^{\mathbf{elem}})^2 + \sum_{e\subset\partial T,\, e\in\mathbb{E}_h(\mathbf{\Omega})} (\eta_{\alpha,e}^{\mathbf{inter}})^2 + \sum_{e\subset\partial T,\, e\in\mathbb{E}_h(\mathbf{\Gamma}_N)} (\eta_{\alpha,e}^{\mathbf{Neum}})^2 \right]^{1/2}. \tag{3.21}$$

In order to estimate the error in the entire mesh $\mathbb{M}_h(\mathbf{\Omega})$, one uses

$$\eta_\alpha := \sqrt{\sum_{T\in\mathbb{M}_h(\mathbf{\Omega})} (\eta_{\alpha,T}^{\mathbf{loc}})^2}. \tag{3.22}$$

We will need $\mathbf{f}_h \in [\mathbb{L}^2(\mathbf{\Omega})]^2$ and $\mathbf{g}_h \in [\mathbb{L}^2(\mathbf{\Gamma}_N)]^2$ such that

$$\mathbf{f}_h|_T := \mathbf{f}_T, \qquad \text{and} \qquad \mathbf{g}_h|_e := \mathbf{g}_e. \tag{3.23}$$

We consider now polynomial inverse estimates in weighted Sobolev spaces. The inverse estimate for the p-version is much more involved than that of the h-version. In the latter, one simply transforms the function onto the reference element. By using a simple norm equivalence, one deduces the results on the reference element which is transformed back to the original element. One has the following polynomial inverse estimates for the unidimensional case. We refer the interested readers to [17, 18, 32, 15, 11, 10] for some pertaining analyses.

LEMMA. *Given α, β such that $-1 < \alpha < \beta$ and some $\delta \in [0,1]$. For every univariate polynomial π_p of degree $p \geq 1$ on the 1D reference element $[0,1]$, one has*

$$\int_0^1 \left[\pi_p(t)\right]^2 \omega_{[0,1]}^{\alpha}(t)dt \;\leq\; C_1 p^{2(\beta-\alpha)} \int_0^1 \left[\pi_p(t)\right]^2 \omega_{[0,1]}^{\beta}(t)dt \tag{3.24}$$

$$\int_0^1 \left[\pi_p'(t)\right]^2 \omega_{[0,1]}^{2\delta}(t)dt \;\leq\; C_2 p^{2(2-\delta)} \int_0^1 \left[\pi_p(t)\right]^2 \omega_{[0,1]}^{\delta}(t)dt \tag{3.25}$$

The constants are $C_1 = C_1(\alpha,\beta)$, $C_2 = C_2(\delta)$ which do not depend on p.

The above weighted polynomial inverse estimates on the unit interval is very complicated. It involves the expansion of a polynomial in Jacobi basis. One uses the eigenvalues of the Jacobi polynomials. To represent the integrals in the Sobolev norms, one expresses them in term of the Gauss-Lobatto quadrature points which have good properties with respect to the Jacobi polynomials.

The following theorem has been documented in [17, 18] for the weight function

$$\omega_{\widehat{T}}(\mathbf{x}) = \text{distance}(\mathbf{x}, \partial\widehat{T}) \qquad \forall\, \mathbf{x} \in \widehat{T} \tag{3.26}$$

which is a bubble function vanishing at the boundary $\partial\widehat{T}$. The advantage of the Gegenbauer weight is that it is not expensive to evaluate in practical computations. In a-posteriori error estimators, the weights need to be explicitly evaluated and this is therefore not only important for theoretical reasons. Moreover, it is conceivable to evaluate some involved integrals analytically instead of using quadrature rules. In addition, the following estimates are interesting by themselves.

From here onward, we use the usual shorthand $X \precsim Y$ if there is a constant c such that $X \leq cY$ in which c is independent on h. In addition, $X \simeq Y$ amounts to $X \precsim Y \precsim X$. We have detailed the analysis of the next result in [20].

LEMMA. *Given α, β such that $-1 < \alpha < \beta$ and some $\delta \in [0,1]$. By using the generalized Gegenbauer weight*

$$\omega_{\widehat{T}}(\mathbf{x}) = \lambda_{0,\widehat{T}}(\mathbf{x})\lambda_{1,\widehat{T}}(\mathbf{x})\lambda_{2,\widehat{T}}(\mathbf{x}) = (1-x_1-x_2)x_1x_2 \tag{3.27}$$

for $\mathbf{x} = (x_1, x_2)$ on the 2D reference element

$$\widehat{T} = \Big\{\mathbf{x} = (x_1,x_2) \in \mathbf{R}^2 : 0 \leq x_1 \leq 1,\ 0 \leq x_2 \leq 1,\ 0 \leq x_1 + x_2 \leq 1\Big\}, \tag{3.28}$$

one has for every bivariate polynomial π_p of degree $p \geq 1$

$$\int_{\widehat{T}} \big[\pi_p(\mathbf{x})\big]^2 \omega_{\widehat{T}}^{\alpha}(\mathbf{x})d\mathbf{x} \ \leq\ C_1 p^{2(\beta-\alpha)} \int_{\widehat{T}} \big[\pi_p(\mathbf{x})\big]^2 \omega_{\widehat{T}}^{\beta}(\mathbf{x})d\mathbf{x} \tag{3.29}$$

$$\int_{\widehat{T}} \big|\nabla\pi_p(\mathbf{x})\big|^2 \omega_{\widehat{T}}^{2\delta}(\mathbf{x})d\mathbf{x} \ \leq\ C_2 p^{2(2-\delta)} \int_{\widehat{T}} \big[\pi_p(\mathbf{x})\big]^2 \omega_{\widehat{T}}^{\delta}(\mathbf{x})d\mathbf{x} \tag{3.30}$$

The constants are $C_1 = C_1(\alpha,\beta)$, $C_2 = C_2(\delta)$ which do not depend on p.

LEMMA *Consider a univariate polynomial π of degree $p \geq 1$ defined on the unit reference interval $\widehat{e} = [0,1]$ and a parameter $0 < \gamma \leq 1$. There exists a bivariate extension $v \in \mathbb{H}^1(\widehat{T})$ defined on the reference triangle $\widehat{T}$ from (3.14) such that it has the next properties w.r.t. the weight $\omega_{\widehat{e}}^{\alpha}$:*

$$v|_{\widehat{e}} \ =\ \pi\omega_{\widehat{e}}^{\alpha} \qquad \textit{and} \qquad v\big|_{(\partial\widehat{T}\setminus\widehat{e})} \equiv 0 \tag{3.31}$$

$$\|v\|^2_{\mathbb{L}_2(\widehat{T})} \ \leq\ C(\alpha)\gamma\|\pi\omega_{\widehat{e}}^{\alpha/2}\|^2_{\mathbb{L}_2(\widehat{e})} \tag{3.32}$$

$$\|\nabla v\|^2_{\mathbb{L}_2(\widehat{T})} \ \leq\ C(\alpha)\big[\gamma p^{2(2-\alpha)} + \gamma^{-1}\big]\|\pi\omega_{\widehat{e}}^{\alpha/2}\|^2_{\mathbb{L}_2(\widehat{e})}. \tag{3.33}$$

THEOREM. *For an element $T \in \mathbb{M}_h(\mathbf{\Omega})$, define the oscillation*

$$\mathrm{OSC}(\mathbf{f},\mathbf{f}_T,\alpha,T) := \|(\mathbf{f}_T - \mathbf{f})\omega_T^{\alpha/2}\|_{[\mathbb{L}_2(T)]^2}. \textit{ One has} \tag{3.34}$$

$$\eta^{\mathbf{elem}}_{\alpha,T} \precsim C_p\|\mathbf{U}-\mathbf{U}_h\|_{[\mathbb{H}^1(T)]^2} + \frac{h(T)}{p}\mathrm{OSC}(\mathbf{f},\mathbf{f}_T,\alpha,T). \tag{3.35}$$

Concerning the edge estimation, introduce the oscillations for $A \subset \mathbf{\Omega}$, $B \subset \mathbf{\Gamma}_N$

$$\mathrm{OSC}(\mathbf{f},\mathbf{f}_h,A) := \|\mathbf{f}-\mathbf{f}_h\|_{[\mathbb{L}^2(A)]^2}, \quad \mathrm{OSC}(\mathbf{g},\mathbf{g}_h,B) := \|\mathbf{g}-\mathbf{g}_h\|_{[\mathbb{L}^2(B)]^2}. \tag{3.36}$$

For a Neumann edge $e \in \mathbb{E}_h(\mathbf{\Gamma}_N)$ incident upon $T_e \in \mathbb{M}_h(\mathbf{\Omega})$,

$$\eta_{\alpha,e}^{\mathbf{Neum}} \precsim C_p \|\mathbf{U}-\mathbf{U}_h\|_{[\mathbb{H}^1(T_e)]^2} + \frac{h(e)}{\sqrt{p}}\mathrm{OSC}(\mathbf{f},\mathbf{f}_h,T_e) + \sqrt{\frac{h(e)}{p}}\mathrm{OSC}(\mathbf{g},\mathbf{g}_h,e). \tag{3.37}$$

For an internal edge $e \in \mathbb{E}_h(\mathbf{\Omega})$,

$$\eta_{\alpha,e}^{\mathbf{inter}} \precsim C_p \|\mathbf{U}-\mathbf{U}_h\|_{[\mathbb{H}^1(\mathcal{N}(e))]^2} + \frac{h(e)}{\sqrt{p}}\mathrm{OSC}(\mathbf{f},\mathbf{f}_h,\mathcal{N}(e)). \tag{3.38}$$

In addition,

$$\|\mathbf{U}-\mathbf{U}_h\|_{[\mathbb{H}^1(\mathbf{\Omega})]^2} \precsim C_p\eta_\alpha \quad + \quad \sum_{T\in\mathbb{M}_h(\mathbf{\Omega})} \frac{h(T)}{p}\mathrm{OSC}(\mathbf{f},\mathbf{f}_T,T) + \tag{3.39}$$

$$\sum_{e\in\mathbb{E}_h(\mathbf{\Gamma}_N)} \sqrt{\frac{h(e)}{p}}\mathrm{OSC}(\mathbf{g},\mathbf{g}_e,e). \tag{3.40}$$

PROOF. Introduce

$$\mathbf{\Psi}_T := \Big[\mathbf{f}_T + \mu\Delta\mathbf{U}_h + (\lambda+\mu)\mathbf{grad}(\mathrm{div}(\mathbf{U}_h))\Big]\omega_T^\alpha. \tag{3.41}$$

We want first to estimate $|\mathbf{\Psi}_T|^2_{[\mathbb{H}^1(T)]^2}$ where

$$|\mathbf{\Psi}_T|^2_{[\mathbb{H}^1(T)]^2} = \sum_j |\nabla\Psi_{T,j}|_{[\mathbb{L}_2(T)]^2} \quad \text{in which} \quad \mathbf{\Psi}_T = [\Psi_{T,1},\Psi_{T,2}]^{\mathrm{T}}. \tag{3.42}$$

In term of the componentwise stress tensor, we have

$$\Psi_{T,j} \;=\; \Big[f_{T,j} + \sum_{i=1}^{2}\partial_i[\sigma_{ij}(\mathbf{U}_h)]\Big]\omega_T^\alpha \tag{3.43}$$

$$\big|\nabla\Psi_{T,j}\big|^2_{[\mathbb{L}_2(T)]^2} \;\precsim\; \int_T \Big[f_{T,j} + \sum_i \partial_i[\sigma_{ij}(\mathbf{U}_h)]\Big]^2\big|\nabla\omega_T^\alpha\big|^2 + \tag{3.44}$$

$$\int_T \Big|\nabla\{f_{T,j} + \sum_i \partial_i[\sigma_{ij}(\mathbf{U}_h)]\}\Big|^2\omega_T^{2\alpha}. \tag{3.45}$$

In order to estimate the term in (3.44), we consider for any $\widehat{\mathbf{x}} = (\widehat{x}_1,\widehat{x}_2) \in \widehat{T}$, one has

$$\big[\partial_1\omega_{\widehat{T}}^\alpha(\widehat{\mathbf{x}})\big]^2 \;=\; \big[(-\alpha)(1-\widehat{x}_1-\widehat{x}_2)^{\alpha-1}\widehat{x}_1^\alpha\widehat{x}_2^\alpha + \alpha(1-\widehat{x}_1-\widehat{x}_2)^\alpha\widehat{x}_1^{\alpha-1}\widehat{x}_2^\alpha\big]^2 \tag{3.46}$$

$$\simeq\; (1-\widehat{x}_1-\widehat{x}_2)^{2(\alpha-1)}\widehat{x}_1^{2\alpha}\widehat{x}_2^{2\alpha} + (1-\widehat{x}_1-\widehat{x}_2)^{2\alpha}\widehat{x}_1^{2(\alpha-1)}\widehat{x}_2^{2\alpha} \tag{3.47}$$

$$\simeq\; \omega_{\widehat{T}}^{2(\alpha-1)}(\widehat{\mathbf{x}})\big[\widehat{x}_1^2\widehat{x}_2^2 + (1-\widehat{x}_1-\widehat{x}_2)^2\widehat{x}_2^2\big] \le 2\omega_{\widehat{T}}^{2(\alpha-1)}(\widehat{\mathbf{x}}). \tag{3.48}$$

With a similar estimate for $\partial_2\omega_{\widehat{T}}^\alpha(\widehat{\mathbf{x}})$, obtain

$$\big|\nabla_{\widehat{\mathbf{x}}}\,\omega_{\widehat{T}}^\alpha(\widehat{\mathbf{x}})\big|^2 \precsim \omega_{\widehat{T}}^{2(\alpha-1)}(\widehat{\mathbf{x}}) \qquad \text{for all} \quad \widehat{\mathbf{x}} \in \widehat{T}. \tag{3.49}$$

With the help of the affine transform $F_T : \widehat{T} \longrightarrow T$, the barycentric coordinates $\lambda_{i,T}(\mathbf{x}) = \lambda_{i,\widehat{T}}(F_T^{-1}(\mathbf{x}))$ for $\mathbf{x} = F_T(\widehat{\mathbf{x}}) \in T$, obtain

$$\left|\nabla_{\mathbf{x}}\,\omega_T^{\alpha}(\mathbf{x})\right|^2 = \left|(\mathbf{D}F_T^{-1})\nabla_{\widehat{\mathbf{x}}}\,\omega_{\widehat{T}}^{\alpha}(\widehat{\mathbf{x}})\right|^2 \precsim \frac{1}{h^2(T)}\left|\nabla_{\widehat{\mathbf{x}}}\,\omega_{\widehat{T}}^{\alpha}(\widehat{\mathbf{x}})\right|^2 \tag{3.50}$$

$$\precsim \frac{1}{h^2(T)}\omega_{\widehat{T}}^{2(\alpha-1)}(\widehat{\mathbf{x}}) = \frac{1}{h^2(T)}\omega_T^{2(\alpha-1)}(\mathbf{x}). \tag{3.51}$$

Hence, for each $j = 1, 2$, we deduce

$$\int_T \Big[f_{T,j} + \sum_i \partial_i[\sigma_{ij}(\mathbf{U}_h)]\Big]^2 \left|\nabla\omega_T^{\alpha}\right|^2 \precsim \frac{1}{h^2(T)}\int_T \Big[f_{T,j} + \sum_i \partial_i[\sigma_{ij}(\mathbf{U}_h)]\Big]^2 \omega_T^{2(\alpha-1)}. \tag{3.52}$$

Apply the polynomial inverse estimate (3.29) and the determinant properties (3.15) to the polynomial $\pi_p := f_{T,j} + \sum_i \partial_i[\sigma_{ij}(\mathbf{U}_h)]$

$$\|\pi_p\omega_T^{(\alpha-1)}\|^2_{\mathbb{L}_2(T)} = \int_{\widehat{T}} \widehat{\pi}_p^2(\widehat{\mathbf{x}})\,\omega_{\widehat{T}}^{2(\alpha-1)}(\widehat{\mathbf{x}})\det|\mathbf{D}F_T(\widehat{\mathbf{x}})|d\widehat{\mathbf{x}} \tag{3.53}$$

$$\precsim h^2(T)p^{2(2-\alpha)}\|\widehat{\pi}_p\omega_{\widehat{T}}^{\alpha/2}\|^2_{\mathbb{L}_2(\widehat{T})} \tag{3.54}$$

$$= h^2(T)p^{2(2-\alpha)}\int_T \pi_p^2(\mathbf{x})\omega_T^{\alpha}(\mathbf{x})\det|\mathbf{D}F_T^{-1}(\mathbf{x})|d\mathbf{x} \tag{3.55}$$

$$\precsim p^{2(2-\alpha)}\|\pi_p\omega_T^{\alpha/2}\|^2_{\mathbb{L}_2(T)}. \tag{3.56}$$

Hence,

$$\int_T \Big[f_{T,j} + \sum_i \partial_i[\sigma_{ij}(\mathbf{U}_h)]\Big]^2 \left|\nabla\omega_T^{\alpha}\right|^2 \precsim \frac{p^{2(2-\alpha)}}{h^2(T)}\int_T \Big[f_{T,j} + \sum_i \partial_i[\sigma_{ij}(\mathbf{U}_h)]\Big]^2 \omega_T^{\alpha}. \tag{3.57}$$

Concerning the term in (3.45), proceed similarly but with respect to the polynomial inverse estimate (3.30) where $\delta \equiv \alpha$ and obtain

$$\int_T \Big|\nabla\{f_{T,j} + \sum_i \partial_i[\sigma_{ij}(\mathbf{U}_h)]\}\Big|^2 \omega_T^{2\alpha} \precsim \frac{p^{2(2-\alpha)}}{h^2(T)}\int_T \Big[f_{T,j} + \sum_i \partial_i[\sigma_{ij}(\mathbf{U}_h)]\Big]^2 \omega_T^{\alpha}. \tag{3.58}$$

By combining the last two estimates for $j = 1, 2$, obtain

$$|\mathbf{\Psi}_T|^2_{[\mathbb{H}^1(T)]^2} \precsim \frac{p^{2(2-\alpha)}}{h^2(T)}\int_T \sum_{j=1}^{2}\Big[f_{T,j} + \sum_i \partial_i[\sigma_{ij}(\mathbf{U}_h)]\Big]^2 \omega_T^{\alpha} \tag{3.59}$$

$$= \frac{p^{2(2-\alpha)}}{h^2(T)}\|\mathbf{\Psi}_T\omega^{-\alpha/2}\|^2_{[\mathbb{L}_2(T)]^2}. \tag{3.60}$$

On the other hand, according to the definition of $\boldsymbol{\Psi}_T$ and by using (3.60), obtain

$$\begin{aligned}
\|\boldsymbol{\Psi}_T\omega^{-\alpha/2}\|^2_{[\mathbb{L}_2(T)]^2} &= \int_T \left|\mathbf{f}_T+\mu\Delta\mathbf{U}_h+(\lambda+\mu)\mathbf{grad}(\mathrm{div}(\mathbf{U}_h))\right|^2\omega_T^{\alpha}\\
&= \int_T \left[\mathbf{f}_T+\mu\Delta\mathbf{U}_h+(\lambda+\mu)\mathbf{grad}(\mathrm{div}(\mathbf{U}_h))\right]^{\mathrm{T}}\boldsymbol{\Psi}_T\\
&= \int_T \omega_T^{\alpha/2}[\mathbf{f}_T-\mathbf{f}]^{\mathrm{T}}\boldsymbol{\Psi}_T\omega_T^{-\alpha/2}+\int_T \boldsymbol{\varepsilon}(\mathbf{U}-\mathbf{U}_h):\boldsymbol{\sigma}(\boldsymbol{\Psi}_T)\\
&\precsim \left\{\|(\mathbf{f}_T-\mathbf{f})\omega_T^{\alpha/2}\|_{[\mathbb{L}_2(T)]^2}+\|\mathbf{U}-\mathbf{U}_h\|_{[\mathbb{H}^1(T)]^2}\frac{p^{(2-\alpha)}}{h(T)}\right\}\times\\
&\quad \|\boldsymbol{\Psi}_T\omega^{-\alpha/2}\|_{[\mathbb{L}_2(T)]^2}.
\end{aligned}$$

The internal estimator verifies

$$\eta_{\alpha,T}^{\mathbf{elem}} = \frac{h(T)}{p}\|\boldsymbol{\Psi}_T\omega^{-\alpha/2}\|_{[\mathbb{L}_2(T)]^2} \tag{3.61}$$

$$\precsim \frac{h(T)}{p}\left\{\frac{p^{(2-\alpha)}}{h(T)}\|\mathbf{U}-\mathbf{U}_h\|_{[\mathbb{H}^1(T)]^2}+\|(\mathbf{f}_T-\mathbf{f})\omega_T^{\alpha/2}\|_{[\mathbb{L}_2(T)]^2}\right\} \tag{3.62}$$

$$\precsim p^{(1-\alpha)}\|\mathbf{U}-\mathbf{U}_h\|_{[\mathbb{H}^1(T)]^2}+\frac{h(T)}{p}\|(\mathbf{f}_T-\mathbf{f})\omega_T^{\alpha/2}\|_{[\mathbb{L}_2(T)]^2} \tag{3.63}$$

yielding (3.35).

For an edge $e\in\mathbb{E}_h(\boldsymbol{\Gamma}_N)$ which is incident upon an element T_e, define the polynomial

$$\mathbf{R}_e := \mathbf{g}_e-\boldsymbol{\sigma}(\mathbf{U}_h)_{|_{T_e}}\mathbf{n}(e). \tag{3.64}$$

Let $\widetilde{\boldsymbol{\theta}}_e$ be the componentwise extension of $\mathbf{R}_e$ according to (3.31) on T_e such that $\widetilde{\boldsymbol{\theta}}_e|_{(\partial T_e\setminus e)}\equiv 0$ and $(\widetilde{\boldsymbol{\theta}}_e)|_e\equiv\mathbf{R}_e\omega_e^{\alpha}$. Define $\boldsymbol{\theta}_e:=\mathbf{R}_e\omega_e^{\alpha}$.

$$\int_e \mathbf{R}_e^{\mathrm{T}}\widetilde{\boldsymbol{\theta}}_e = \int_e \mathbf{g}_e^T\widetilde{\boldsymbol{\theta}}_e-\int_e(\boldsymbol{\sigma}(\mathbf{U}_h)_{|_{T_e}}\mathbf{n}(e))^{\mathrm{T}}\widetilde{\boldsymbol{\theta}}_e \tag{3.65}$$

$$= \underbrace{\int_e(\mathbf{g}_e-\mathbf{g})^T\widetilde{\boldsymbol{\theta}}_e}_{(a)}+\underbrace{\int_e\mathbf{g}^T\widetilde{\boldsymbol{\theta}}_e-\int_e(\boldsymbol{\sigma}(\mathbf{U}_h)_{|_{T_e}}\mathbf{n}(e))^{\mathrm{T}}\widetilde{\boldsymbol{\theta}}_e}_{(b)}. \tag{3.66}$$

$$(a) = \int_e(\mathbf{g}_e-\mathbf{g})^T\mathbf{R}_e\omega_e^{\alpha}=\int_e\left[(\mathbf{g}_e-\mathbf{g})\omega_e^{\alpha/2}\right]^T\left[(\mathbf{R}_e\omega_e^{\alpha})\omega_e^{-\alpha/2}\right] \tag{3.67}$$

$$= \int_e\left[(\mathbf{g}_e-\mathbf{g})\omega_e^{\alpha/2}\right]^T\left[\boldsymbol{\theta}_e\omega_e^{-\alpha/2}\right] \tag{3.68}$$

$$\leq \|(\mathbf{g}_e-\mathbf{g})\omega_e^{\alpha/2}\|_{[\mathbb{L}_2(e)]^2}\|\boldsymbol{\theta}_e\omega_e^{-\alpha/2}\|_{[\mathbb{L}_2(e)]^2}. \tag{3.69}$$

As for (b), we proceed as follows. Since $\widetilde{\boldsymbol{\theta}}_e$ vanishes on $\partial T_e \setminus \boldsymbol{\Gamma}_N$, we have

$$\int_e (\boldsymbol{\sigma}(\mathbf{U}_h)_{|_{T_e}}\mathbf{n}(e))^{\mathrm{T}}\widetilde{\boldsymbol{\theta}}_e = \int_{T_e} \boldsymbol{\varepsilon}(\mathbf{U}_h) : \boldsymbol{\sigma}(\widetilde{\boldsymbol{\theta}}_e) + \tag{3.70}$$

$$\int_{T_e} \{\mu\Delta\mathbf{U}_h + (\mu+\lambda)\mathbf{grad}(\mathrm{div}(\mathbf{U}_h))\}^{\mathrm{T}}\widetilde{\boldsymbol{\theta}}_e. \tag{3.71}$$

Similarly,

$$\int_e \mathbf{g}^{\mathrm{T}}\widetilde{\boldsymbol{\theta}}_e = \int_{T_e} \boldsymbol{\varepsilon}(\mathbf{U}) : \boldsymbol{\sigma}(\widetilde{\boldsymbol{\theta}}_e) + \int_{T_e} \mathbf{f}^{\mathrm{T}}\widetilde{\boldsymbol{\theta}}_e. \tag{3.72}$$

Hence,

$$\begin{aligned}
(b) &= \int_{T_e} \boldsymbol{\varepsilon}(\mathbf{U}_h - \mathbf{U}) : \boldsymbol{\sigma}(\widetilde{\boldsymbol{\theta}}_e) + \int_{T_e} \{\mathbf{f} + \mu\Delta\mathbf{U}_h + (\mu+\lambda)\mathbf{grad}(\mathrm{div}\,\mathbf{U}_h)\}^{\mathrm{T}}\widetilde{\boldsymbol{\theta}}_e \\
&\leq \Big[\int_{T_e} \boldsymbol{\varepsilon}(\mathbf{U}_h - \mathbf{U}) : \boldsymbol{\sigma}(\mathbf{U}_h - \mathbf{U})\Big]^{1/2}\Big[\int_{T_e} \boldsymbol{\varepsilon}(\widetilde{\boldsymbol{\theta}}_e) : \boldsymbol{\sigma}(\widetilde{\boldsymbol{\theta}}_e)\Big]^{1/2} + \\
&\quad \big\|\mathbf{f} + \mu\Delta\mathbf{U}_h + (\mu+\lambda)\mathbf{grad}(\mathrm{div}\,\mathbf{U}_h)\big\|_{[\mathbb{L}_2(T_e)]^2}\big\|\widetilde{\boldsymbol{\theta}}_e\big\|_{[\mathbb{L}_2(T_e)]^2} \\
&\precsim \|\mathbf{U} - \mathbf{U}_h\|_{[\mathbb{H}^1(T_e)]^2}\|\widetilde{\boldsymbol{\theta}}_e\|_{[\mathbb{H}^1(T_e)]^2} + \\
&\quad \big\|\mathbf{f} + \mu\Delta\mathbf{U}_h + (\mu+\lambda)\mathbf{grad}(\mathrm{div}\,\mathbf{U}_h)\big\|_{[\mathbb{L}_2(T_e)]^2}\big\|\widetilde{\boldsymbol{\theta}}_e\big\|_{[\mathbb{L}_2(T_e)]^2}.
\end{aligned}$$

According to the properties (3.32) and (3.33) of the extension operator componentwise,

$$\|\widetilde{\boldsymbol{\theta}}_e\|^2_{[\mathbb{L}_2(T_e)]^2} \precsim h(T_e)\gamma\|\boldsymbol{\theta}_e\omega_e^{-\alpha/2}\|^2_{[\mathbb{L}_2(e)]^2} \tag{3.73}$$

$$|\widetilde{\boldsymbol{\theta}}_e|^2_{[\mathbb{H}^1(T_e)]^2} \precsim \frac{1}{h(T_e)}(\gamma p^{2(2-\alpha)} + \gamma^{-1})\|\boldsymbol{\theta}_e\omega_e^{-\alpha/2}\|^2_{[\mathbb{L}_2(e)]^2}. \tag{3.74}$$

Hence,

$$\begin{aligned}
(b) \precsim \Big\{&\|\mathbf{U} - \mathbf{U}_h\|_{[\mathbb{H}^1(T_e)]^2}\Big[\frac{1}{h(T_e)}(\gamma p^{2(2-\alpha)} + \gamma^{-1})\Big]^{1/2} + \\
&\big\|\mathbf{f} + \mu\Delta\mathbf{U}_h + (\mu+\lambda)\mathbf{grad}(\mathrm{div}\,\mathbf{U}_h)\big\|_{[\mathbb{L}_2(T_e)]^2}\sqrt{h(T_e)\gamma}\Big\}\|\boldsymbol{\theta}_e\omega_e^{-\alpha/2}\|_{[\mathbb{L}_2(e)]^2}.
\end{aligned}$$

On the other hand,

$$\int_e \mathbf{R}_e^{\mathrm{T}}\,\widetilde{\boldsymbol{\theta}}_e = \int_e |\mathbf{R}_e|^2\omega_e^{\alpha} = \int_e |\boldsymbol{\theta}_e|^2\omega_e^{-\alpha} = \|\boldsymbol{\theta}_e\omega_e^{-\alpha/2}\|^2_{[\mathbb{L}_2(e)]^2}. \tag{3.75}$$

By combining that with the estimates of (a) and (b), and by cancelling on both sides with $\|\boldsymbol{\theta}_e\omega_e^{-\alpha/2}\|_{[\mathbb{L}_2(e)]^2}$, obtain

$$\|\boldsymbol{\theta}_e\omega_e^{-\alpha/2}\|_{[\mathbb{L}_2(e)]^2} \precsim \|(\mathbf{g}_e - \mathbf{g})\omega_e^{\alpha/2}\|_{[\mathbb{L}_2(e)]^2} + \tag{3.76}$$

$$\|\mathbf{U} - \mathbf{U}_h\|_{[\mathbb{H}^1(T_e)]^2}\Big[\frac{1}{h(T_e)}(\gamma p^{2(2-\alpha)} + \gamma^{-1})\Big]^{1/2} + \tag{3.77}$$

$$\big\|\mathbf{f} + \mu\Delta\mathbf{U}_h + (\mu+\lambda)\mathbf{grad}(\mathrm{div}\,\mathbf{U}_h)\big\|_{[\mathbb{L}_2(T_e)]^2}\sqrt{h(T_e)\gamma}. \tag{3.78}$$

Since the Neumann edge estimator $\eta_{\alpha,e}^{\mathbf{Neum}} = \sqrt{h(e)/(2p)}\|\boldsymbol{\theta}_e\omega_e^{-\alpha/2}\|_{[\mathbb{L}_2(e)]^2}$ and by using $h(e) \simeq h(T_e)$ due to shape regularity, obtain

$$\eta_{\alpha,e}^{\mathbf{Neum}} \leq C_p\|\mathbf{U}-\mathbf{U}_h\|_{[\mathbb{H}^1(T_e)]^2} + \frac{h(T_e)}{\sqrt{p}}\mathrm{OSC}(\mathbf{f},\mathbf{f}_{T_e}) + \sqrt{\frac{h(e)}{p}}\mathrm{OSC}(\mathbf{g},\mathbf{g}_e) \tag{3.79}$$

which provides (3.37).

The case of an internal edge $e \in \mathbb{E}_h(\boldsymbol{\Omega})$ incident upon $T_{(1,e)}$ and $T_{(2,e)}$ is treated in a similar manner. But use the next vector-valued polynomial instead of (3.64)

$$\mathbf{R}_e := \boldsymbol{\sigma}(\mathbf{U}_h)_{|_{T_{(1,e)}}}\mathbf{n}(e) - \boldsymbol{\sigma}(\mathbf{U}_h)_{|_{T_{2,e}}}\mathbf{n}(e). \tag{3.80}$$

For any $\mathbf{W} \in [H^1_{\boldsymbol{\Gamma}_N}(\boldsymbol{\Omega})]^2$

$$\begin{aligned}
R &:= \int_{\boldsymbol{\Omega}} \boldsymbol{\varepsilon}(\mathbf{U}-\mathbf{U}_h) : \boldsymbol{\sigma}(\mathbf{W}) \\
&= \int_{\boldsymbol{\Omega}} \mathbf{f}^{\mathrm{T}}\mathbf{W} + \int_{\boldsymbol{\Gamma}_N} \mathbf{g}^{\mathrm{T}}\mathbf{W} + \sum_{T\in\mathbb{M}_h(\boldsymbol{\Omega})} \Big\{ \int_{\partial T} -[\boldsymbol{\sigma}(\mathbf{U}_h)\mathbf{n}]^T\mathbf{W} \\
&\quad + \int_T [\mu\Delta\mathbf{U}_h + (\lambda+\mu)\mathbf{grad}(\mathrm{div}\mathbf{U}_h)]^{\mathrm{T}}\mathbf{W}\Big\} \\
&= \sum_{T\in\mathbb{M}_h(\boldsymbol{\Omega})} \int_T [\mathbf{f} + \mu\Delta\mathbf{U}_h + (\lambda+\mu)\mathbf{grad}(\mathrm{div}\mathbf{U}_h)]^{\mathrm{T}}\mathbf{W} \\
&\quad + \sum_{e\in\mathbb{E}_h(\boldsymbol{\Gamma}_N)} \int_e \mathbf{g}^T\mathbf{W} - \sum_{e\in\mathbb{E}_h(\boldsymbol{\Gamma}_N)} \int_e \Big[\boldsymbol{\sigma}(\mathbf{U}_h)|_{T_e}\mathbf{n}(e)\Big]^T\mathbf{W} \\
&\quad + \sum_{e\in\mathbb{E}_h(\boldsymbol{\Omega})} \int_e \Big[\boldsymbol{\sigma}(\mathbf{U}_h)|_{T_{(1,e)}}\mathbf{n}(e) - \boldsymbol{\sigma}(\mathbf{U}_h)|_{T_{(2,e)}}\mathbf{n}(e)\Big]^T\mathbf{W}.
\end{aligned}$$

In particular, for $\mathbf{W} = (\mathbf{U}-\mathbf{U}_h) - \mathbf{I}_{h,p}(\mathbf{U}-\mathbf{U}_h)$ where $\mathbf{I}_{h,p}$ is the componentwise Clément interpolant [17, 18], one has in term of the energy norm (2.7)

$$\begin{aligned}
|||\mathbf{U}-\mathbf{U}_h|||_E^2 \precsim\ & \sum_{T\in\mathbb{M}_h(\boldsymbol{\Omega})} \|\mathbf{f}_T + \mu\Delta\mathbf{U}_h + (\lambda+\mu)\mathbf{grad}(\mathrm{div}\mathbf{U}_h)\|_{[\mathbb{L}_2(T)]^2}\|\mathbf{W}\|_{[\mathbb{L}_2(T)]^2} + \\
& \sum_{e\in\mathbb{E}_h(\boldsymbol{\Gamma}_N)} \|\mathbf{g}_e - \boldsymbol{\sigma}(\mathbf{U}_h)|_{T_e}\mathbf{n}(e)\|_{[\mathbb{L}_2(e)]^2}\|\mathbf{W}\|_{[\mathbb{L}_2(e)]^2} + \\
& \sum_{e\in\mathbb{E}_h(\boldsymbol{\Omega})} \|\boldsymbol{\sigma}(\mathbf{U}_h)|_{T_{(1,e)}}\mathbf{n}(e) - \boldsymbol{\sigma}(\mathbf{U}_h)|_{T_{(2,e)}}\mathbf{n}(e)\|_{[\mathbb{L}_2(e)]^2}\|\mathbf{W}\|_{[\mathbb{L}_2(e)]^2} + \\
& \sum_{T\in\mathbb{M}_h(\boldsymbol{\Omega})} \|\mathbf{f}-\mathbf{f}_T\|_{[\mathbb{L}_2(T)]^2}\|\mathbf{W}\|_{[\mathbb{L}_2(T)]^2} + \sum_{e\in\mathbb{E}_h(\boldsymbol{\Gamma}_N)} \|\mathbf{g}-\mathbf{g}_e\|_{[\mathbb{L}_2(e)]^2}\|\mathbf{W}\|_{[\mathbb{L}_2(e)]^2}.
\end{aligned}$$

By using the properties of $\mathbf{I}_{h,p}$, one deduces $\|\mathbf{W}\|_{[\mathbb{L}_2(T)]^2} \precsim \frac{h(T)}{p}\|\mathbf{U}-\mathbf{U}_h\|_{[\mathbb{H}^1(\mathcal{N}(T))]^2}$ for an element T, $\|\mathbf{W}\|_{[\mathbb{L}_2(e)]^2} \precsim \sqrt{\frac{h(e)}{p}}\|\mathbf{U}-\mathbf{U}_h\|_{[\mathbb{H}^1(\mathcal{N}(e))]^2}$ for $e \in \mathbb{E}_h(\boldsymbol{\Omega})$, $\|\mathbf{W}\|_{[\mathbb{L}_2(e)]^2} \precsim$

$\sqrt{\frac{h(e)}{p}}\|\mathbf{U}-\mathbf{U}_h\|_{[\mathbb{H}^1(T_e)]^2}$ for $e\in\mathbb{E}_h(\mathbf{\Gamma}_N)$. Use the fact that both $\mathcal{N}(T)$ and $\mathcal{N}(e)$ contain a few number of elements as well as the equivalence (2.8), to obtain

$$\begin{aligned}\|\mathbf{U}-\mathbf{U}_h\|_{[\mathbb{H}^1(\mathbf{\Omega})]^2} \quad \precsim \quad & \sum_{T\in\mathbb{M}_h(\mathbf{\Omega})}\frac{h(T)}{p}\|\mathbf{f}-\mathbf{f}_T\|_{[\mathbb{L}_2(T)]^2}+\sum_{e\in\mathbb{E}_h(\mathbf{\Gamma}_N)}\sqrt{\frac{h(e)}{p}}\|\mathbf{g}-\mathbf{g}_e\|_{[\mathbb{L}_2(e)]^2}+\\ & \sum_{T\in\mathbb{M}_h(\mathbf{\Omega})}\Big\{\frac{h^2(T)}{p^2}\|\mathbf{f}_T+\mu\Delta\mathbf{U}_h+(\lambda+\mu)\mathbf{grad}(\mathrm{div}\mathbf{U}_h)\|^2_{[\mathbb{L}_2(T)]^2}+\\ & \sum_{e\subset T,e\in\mathbb{E}_h(\mathbf{\Gamma}_N)}\frac{h(e)}{p}\|\mathbf{g}_e-\boldsymbol{\sigma}(\mathbf{U}_h)|_{T_e}\mathbf{n}(e)\|^2_{[\mathbb{L}_2(e)]^2}+\\ & \sum_{e\subset T,e\in\mathbb{E}_h(\mathbf{\Omega})}\frac{h(e)}{p}\|\boldsymbol{\sigma}(\mathbf{U}_h)|_{T_{(1,e)}}\mathbf{n}(e)-\boldsymbol{\sigma}(\mathbf{U}_h)|_{T_{(2,e)}}\mathbf{n}(e)\|^2_{[\mathbb{L}_2(e)]^2}\Big\}^{1/2}\end{aligned}$$

which provides the result for the weight-free case ($\omega_T^\alpha\equiv 1$). As for the weight-based case ($\alpha\neq 0$), apply the polynomial inverse estimate (3.29) componentwise to the vector valued polynomial $\boldsymbol{\pi}_p:=\mathbf{f}_T+\mu\Delta\mathbf{U}_h+(\lambda+\mu)\mathbf{grad}(\mathrm{div}\mathbf{U}_h)$ to obtain

$$\|\boldsymbol{\pi}_p\|_{[\mathbb{L}_2(T)]^2}\precsim p^\alpha\|\boldsymbol{\pi}_p\omega_T^{\alpha/2}\|_{[\mathbb{L}_2(T)]^2} \tag{3.81}$$

and a similar estimate for $\boldsymbol{\pi}_p:=\mathbf{g}_e-\boldsymbol{\sigma}(\mathbf{U}_h)|_{T_e}\mathbf{n}(e)$ and $\boldsymbol{\pi}_p:=\boldsymbol{\sigma}(\mathbf{U}_h)|_{T_{(1,e)}}\mathbf{n}(e)-\boldsymbol{\sigma}(\mathbf{U}_h)|_{T_{(2,e)}}\mathbf{n}(e)$ which are polynomials.

$$\begin{aligned}\|\mathbf{U}-\mathbf{U}_h\|_{[\mathbb{H}^1(\mathbf{\Omega})]^2} \quad \precsim \quad & C_p\sum_{T\in\mathbb{M}_h(\mathbf{\Omega})}\Big[(\eta^{\mathbf{elem}}_{\alpha,T})^2+\sum_{e\subset\partial T,\,e\in\mathbb{E}_h(\mathbf{\Omega})}(\eta^{\mathbf{inter}}_{\alpha,e})^2+\\ & \sum_{e\subset\partial T,\,e\in\mathbb{E}_h(\mathbf{\Gamma}_N)}(\eta^{\mathbf{Neum}}_{\alpha,e})^2\Big]^{1/2}+\\ & \sum_{T\in\mathbb{M}_h(\mathbf{\Omega})}\frac{h(T)}{p}\|\mathbf{f}-\mathbf{f}_T\|_{[\mathbb{L}_2(T)]^2}+\sum_{e\in\mathbb{E}_h(\mathbf{\Gamma}_N)}\sqrt{\frac{h(e)}{p}}\|\mathbf{g}-\mathbf{g}_e\|_{[\mathbb{L}_2(e)]^2}\end{aligned}$$

■

4. Numerical experiments

We would like to present now some practical results of the method which has been elaborated earlier. First, we present our software by using a Neumann solution which does not require any adaptivity. Then, we compare the advantage of the adaptive refinements over the uniform refinements. We consider three benchmarks: punctual accumulation, internal layer and a re-entrant corner. That will be followed by a comparison of the a-posteriori error estimate and the exact accuracy. The first computation involving Neumann boundary consists in computing the errors $\big\|\mathbf{U}-\mathbf{U}_h\big\|_{[\mathbb{L}_2(\mathbf{\Omega})]^2}$, $\big\|\boldsymbol{\varepsilon}-\boldsymbol{\varepsilon}_h\big\|_{[\mathbb{L}_2(\mathbf{\Omega})]^{2\times 2}}$, $\big\|\boldsymbol{\sigma}-\boldsymbol{\sigma}_h\big\|_{[\mathbb{L}_2(\mathbf{\Omega})]^{2\times 2}}$ where $\big\|\boldsymbol{\varepsilon}-\boldsymbol{\varepsilon}_h\big\|^2_{[\mathbb{L}_2(\mathbf{\Omega})]^{2\times 2}}=\sum_{i,j}\big\|\varepsilon_{ij}(\mathbf{U})-\varepsilon_{ij}(\mathbf{U}_h)\big\|^2_{\mathbb{L}_2(\mathbf{\Omega})}$ and the stress

p	LEVEL	$\left\|\mathbf{U}-\mathbf{U}_h\right\|_{[\mathbb{L}_2(\mathbf{\Omega})]^2}$	$\left\|\mathbf{U}-\mathbf{U}_h\right\|_{[\mathbb{H}_1(\mathbf{\Omega})]^2}$	$\left\|\boldsymbol{\varepsilon}-\boldsymbol{\varepsilon}_h\right\|_{[\mathbb{L}_2(\mathbf{\Omega})]^{2\times 2}}$	$\left\|\boldsymbol{\sigma}-\boldsymbol{\sigma}_h\right\|_{[\mathbb{L}_2(\mathbf{\Omega})]^{2\times 2}}$
1	1	2.810669E-02	5.044495E-01	4.142901E-01	1.276802E+00
	2	9.126148E-03	2.862700E-01	2.357796E-01	7.334883E-01
	3	2.543100E-03	1.469115E-01	1.210027E-01	3.768303E-01
	4	6.725183E-04	7.379494E-02	6.087895E-02	1.897894E-01
	5	1.718359E-04	3.692003E-02	3.048486E-02	9.508051E-02
2	1	5.234808E-03	1.492019E-01	1.312249E-01	4.560386E-01
	2	7.247347E-04	4.076179E-02	3.495338E-02	1.177358E-01
	3	9.454467E-05	1.063086E-02	9.065360E-03	3.017947E-02
	4	1.203265E-05	2.700465E-03	2.299566E-03	7.621269E-03
	5	1.536082E-06	6.796863E-04	5.783773E-04	1.912933E-03
3	1	6.524310E-04	2.689130E-02	2.331598E-02	7.974549E-02
	2	4.717494E-05	3.814694E-03	3.276546E-03	1.108150E-02
	3	7.209782E-06	5.138192E-04	4.275579E-04	1.436194E-03
	4	2.918250E-06	1.264953E-04	7.348972E-05	2.127372E-04
	5	1.047373E-06	6.405331E-05	3.000157E-05	6.890122E-05

TABLE 4.1. Neumann situation where adaptivity is not needed: increasing levels.

accuracy is computed similarly. The exact solution is $\mathbf{U}(\mathbf{x}) = [u(\mathbf{x}), u(\mathbf{x})]^T$ such that $u(\mathbf{x}) = (x-1)(y-1)\exp[-10(x^2+y^2)]$. The Neumann boundary consists of $\mathbf{\Gamma}_N := \big(\{0\}\times[0,1]\big)\cup\big([0,1]\times\{0\}\big)$ while the Dirichlet one is $\mathbf{\Gamma}_D := \big(\{1\}\times[0,1]\big)\cup\big([0,1]\times\{1\}\big)$. The expressions of the right hand side $\mathbf{f}$, the exact strain tensor $\boldsymbol{\varepsilon}$ as well as the stress tensor $\boldsymbol{\sigma}$ are computed according to (2.1), (2.2) and (2.3). The results are collected in Table 4.1 where we use polynomial degrees one till three. One incrementation of the FEM-level amounts to a full refinement of the whole mesh. For each polynomial degree, the FEM-level ranges from one to five while the Lamé constants are $(\lambda, \mu) = (2.0, 0.75)$. By using the same Lamé coefficients, our next test consists in investigating the software for the case of increasing polynomial degree. The corresponding results are collected in Table 4.2 where the polynomial degree ranges from one to six. Both simulations for Neumann problem show the performance of our software. There is no need for adaptivity because a global refinement provides a satisfactory convergence and the exact solution does not reflect any special feature. Both the accuracies of the strain and stress are a little worse than that of the displacement because the expressions of the stress

p	$\left\|\mathbf{U}-\mathbf{U}_h\right\|_{[\mathbb{L}_2(\mathbf{\Omega})]^2}$	$\left\|\mathbf{U}-\mathbf{U}_h\right\|_{[\mathbb{H}_1(\mathbf{\Omega})]^2}$	$\left\|\boldsymbol{\varepsilon}-\boldsymbol{\varepsilon}_h\right\|_{[\mathbb{L}_2(\mathbf{\Omega})]^{2\times 2}}$	$\left\|\boldsymbol{\sigma}-\boldsymbol{\sigma}_h\right\|_{[\mathbb{L}_2(\mathbf{\Omega})]^{2\times 2}}$
1	2.063475E-02	4.316495E-01	3.555048E-01	1.102327E+00
2	2.780205E-03	9.851650E-02	8.580540E-02	2.946272E-01
3	2.847784E-04	1.444379E-02	1.239231E-02	4.206869E-02
4	6.058306E-05	2.476896E-03	2.113818E-03	7.378988E-03
5	1.981070E-05	4.525102E-04	3.061656E-04	1.001234E-03
6	7.297680E-06	1.468008E-04	7.031744E-05	1.881655E-04

TABLE 4.2. Neumann situation where adaptivity is not needed: increasing polynomial degrees.

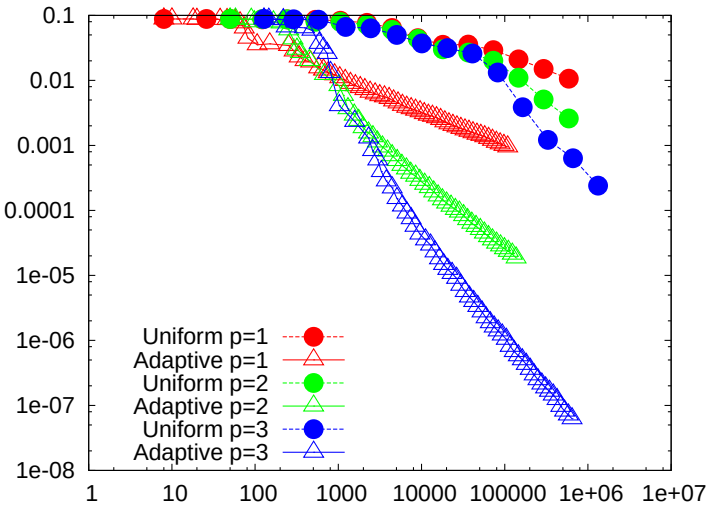

FIGURE 1. $\mathbf{H}^1$-accuracy in function of DOF by using the elastic properties $(\lambda,\mu)=(5,1.25)$. Comparison of uniform and adaptive refinements for $p=1,2,3$ for punctual accumulation.

and the strain involve partial derivatives of the displacements as appearing in (2.1) and (2.2).

The purpose of the next test is to show the numerical performance of our a-posteriori error estimator when coupled with adaptivity using several polynomial degrees. To that end, we consider three test problems: a punctual accumulation, an internal layer, and a re-entrant corner. We always start from a coarse mesh which will then be further refined adaptively. Our adaptive refinement follows the usual method [29, 4, 5]: (1)compute estimator, (2)mark elements, (3)apply refinements. During each refinement, ten percent of the elements admitting the worst a-posteriori error estimates η_α of formula (3.22) are marked to be refined. We adopt the bisection [4, 5] as a refinement technique because

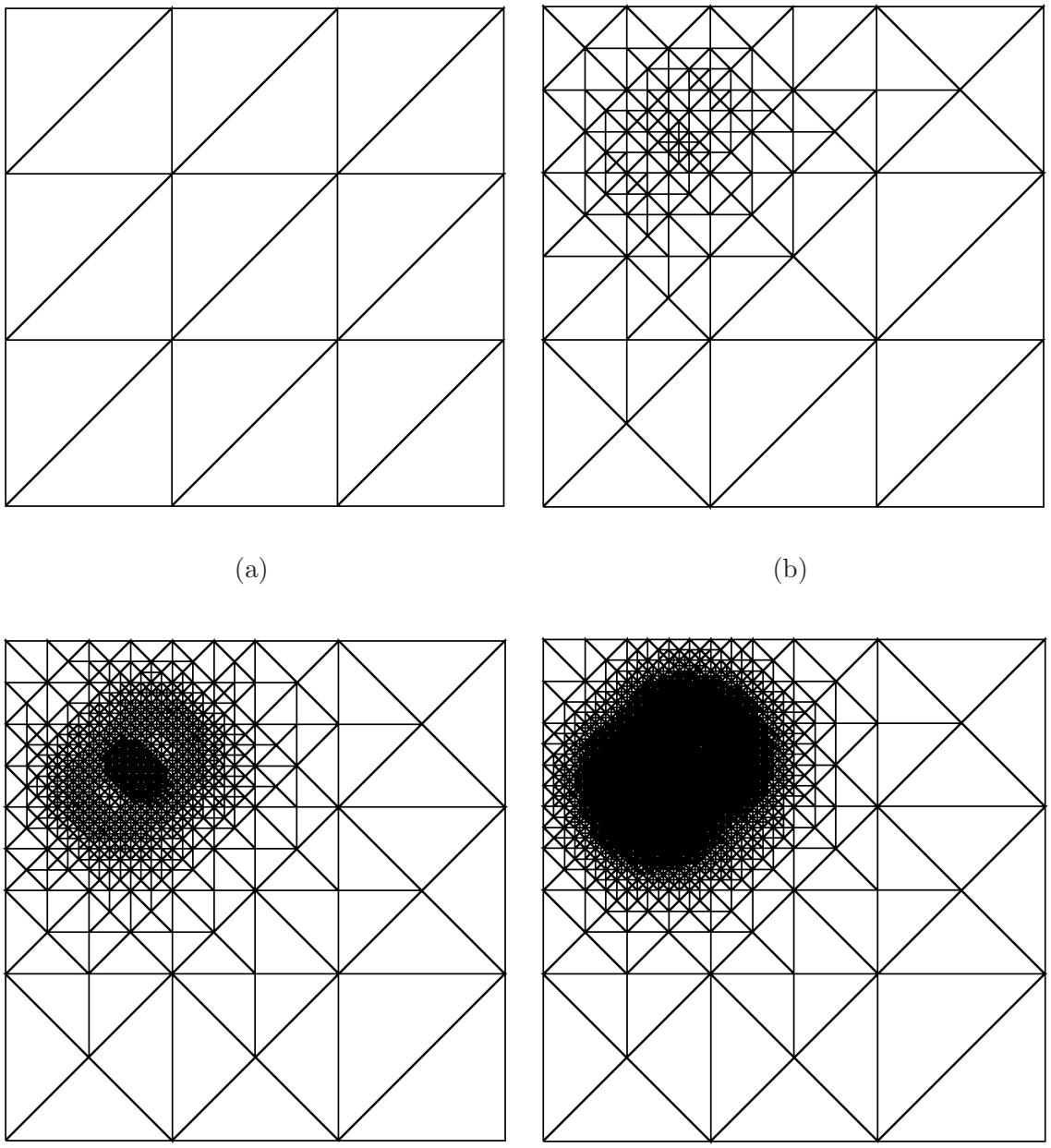

(a) (b)

(c) (d)

FIGURE 2. Refinement history for punctual accumulation where $p = 1$ and $\eta_\alpha = \eta_{0.5}$ for $(\lambda, \mu) = (5, 1.25)$.

that method can be coupled with a fast multilevel higher order linear solver which will be described in a forthcoming paper. For the purpose of this paper, other refinement techniques such as the red-green refinement [8] would operate equally well.

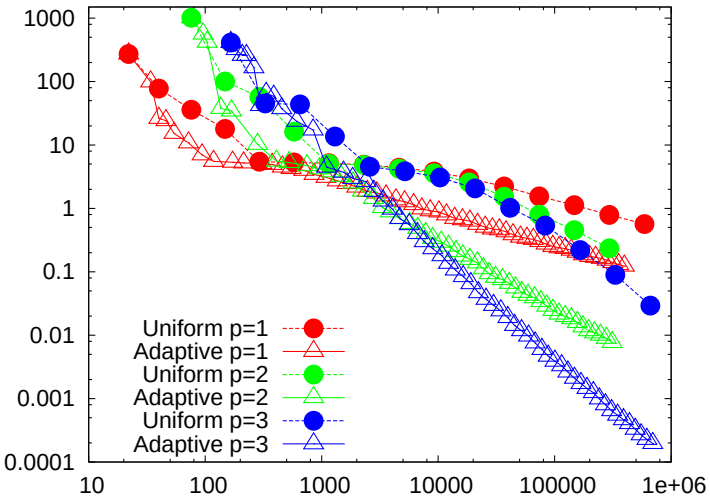

FIGURE 3. $\mathbf{H}^1$-accuracy in function of DOF by using the elastic properties $(\lambda, \mu) = (2, 1)$. Comparison of uniform and adaptive refinements for $p = 1, 2, 3$ for internal layer

In the punctual accumulation, we consider the exact solution in both coordinates

$$x(x-1)y(y-1)\exp\big[-\beta((x-a)^2+(y-b)^2)\big] \tag{4.82}$$

where β is an adjustable large positive parameter. This simulation consists of a purely homogeneous Dirichlet problem, i.e. the Neumann boundary is empty. For a point (x, y) far from (a, b), that function has a small value. The value of β determines the sharpness and the width of the punctual accumulation. As β becomes larger, the width of the accumulation grows smaller and its slope becomes sharper. The accumulation point is situated at $(a, b) = (0.25, 0.75)$ in all tests. We consider the situation in which $\beta = 1.0E + 4$ and we set the elastic material properties to be $(\lambda, \mu) = (5, 1.25)$. We take the estimator η_α where $\alpha = 0.5$ and we consider the polynomial degrees $p = 1, 2, 3$. Our next purpose is to compare the uniform refinements and the adaptive ones. The degree of freedom (DOF) is used as a common reference measurement for all the computational tests. The outcome of the simulation is plotted in Fig. 1 which displays the absolute $\mathbf{H}^1$-accuracy in term of the degree of freedom. The starting mesh consists of a tensor product grid having 18 elements. The advantage of adaptivity over the uniform refinements is as follows. For the polynomial degrees $p = 1, 2, 3$, we need 588290, 588290, 1324802 DOFs to achieve the accuracies of $1.063621E{-}02$, $2.591986E{-}03$, $2.404479E - 04$ respectively in the case of uniform refinements. In contrast, the adaptive case requires only 108738, 136882, 645146 DOFs to produce more precise accuracies $9.490625E - 04$, $1.852298E - 05$, $6.224150E - 08$. In addition, we perceive that for the elastic material property $(\lambda, \mu) = (5, 1.25)$, the use of higher order FEM

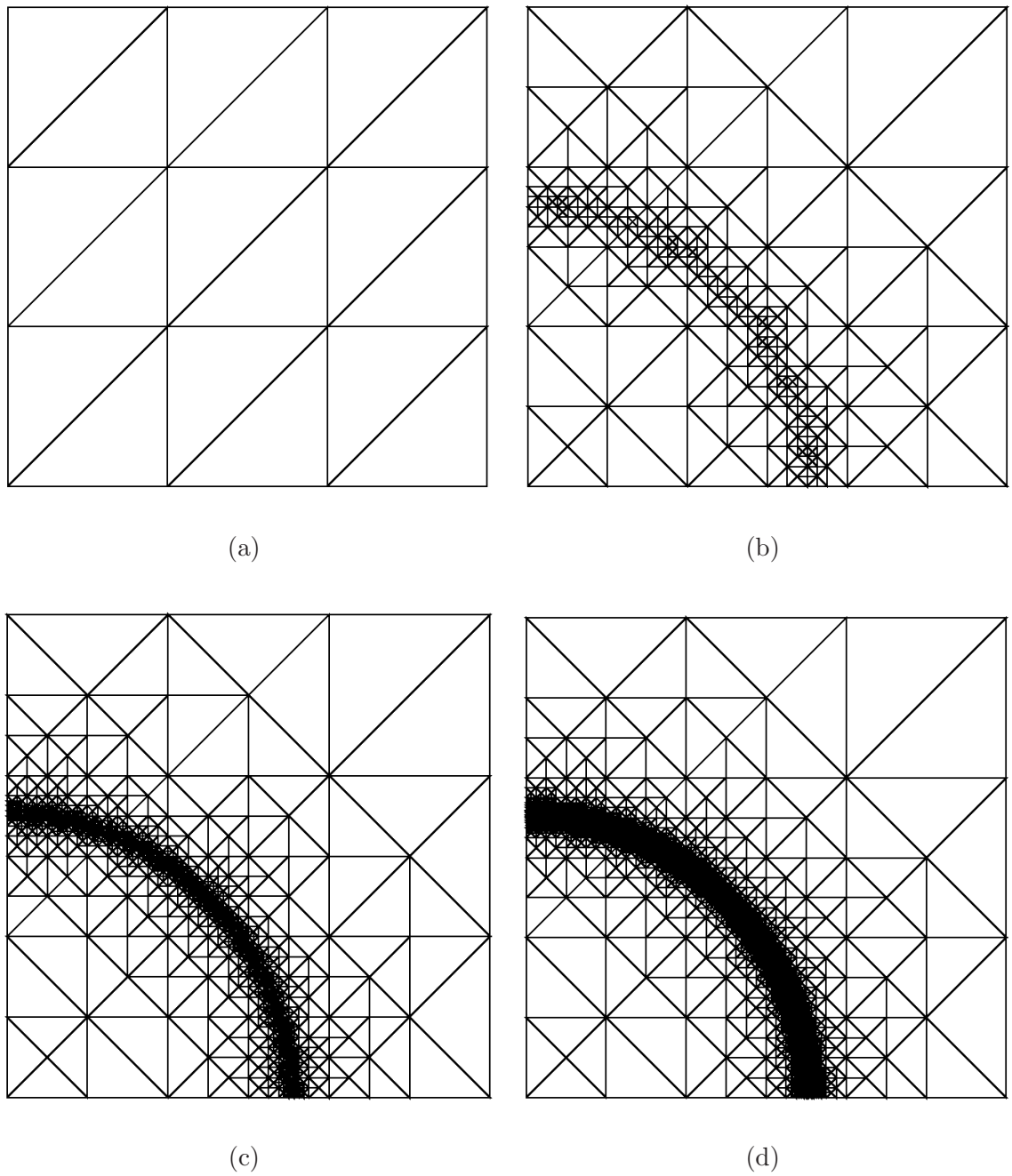

(a) (b)

(c) (d)

FIGURE 4. Refinement history for Neumann with an internal layer where $p = 2$ and $\eta_\alpha = \eta_{0.5}$, $(\lambda, \mu) = (2, 1)$.

$(p \geq 2)$ already proves more advantageous than the piecewise linear $(p = 1)$ setting although that material can still be categorized as absolutely compressible. Indeed, for comparable DOF$\approx$ 100000, the adaptive simulations using $p = 1, 2, 3$ yield respectively the accuracies of $9.490625E-04$ (DOF=108738), $2.576346E-05$ (DOF=99282) and

$1.039906E-06$ (DOF=104444). As observed in Fig. 1, that advantage of higher order computation over the piecewise linear case is also plainly perceived in the uniform case. An instance of the refinement history of the adaptive simulation is displayed in Fig. 2 where we consider the case $\beta = 1.0E+3$ and $p = 1$. The meshes contain respectively 18, 208, 2022 and 12960 elements. It is observed that the position of the punctual accumulation is well captured by the a-posteriori error estimator.

We want now to study a Neumann problem consisting of an internal layer for which the domain $\mathbf{\Omega}$ is again the unit square. The components of the exact solution are chosen to be:

$$(x-1)(y-1)\exp\big[-\beta(\sqrt{(x-a)^2+(y-b)^2}-r_0)^2\big] \tag{4.83}$$

That exact solution uses the distance of $r=\sqrt{(x-a)^2+(y-b)^2}$ from a point (a,b) located outside the domain $\mathbf{\Omega}$. When that distance approaches $r_0>0$, the function presents a layer. The shape of the internal layer is thus the intersection of $\mathbf{\Omega}$ with a circle centered at (a,b) having radius r_0. The point (a,b) is not situated inside $\mathbf{\Omega}$ in order to avoid non-smoothness. In fact, the differentiations contain the next terms which are non-smooth at $(x,y)=(a,b)$:

$$\frac{(x-a)(r-r_0)}{\sqrt{(x-a)^2+(y-b)^2}}\exp[-\beta(r-r_0)^2] \tag{4.84}$$

$$\frac{(y-b)(r-r_0)}{\sqrt{(x-a)^2+(y-b)^2}}\exp[-\beta(r-r_0)^2]. \tag{4.85}$$

That location beyond $\mathbf{\Omega}$ is important to facilitate the computation of the right hand side integration as well as the $\mathbf{H}^1$-accuracies. The top and right sides correspond to the homogeneous Dirichlet boundary $\mathbf{\Gamma}_D$, whereas the left and bottom sides to the Neumann boundary $\mathbf{\Gamma}_N$. The size and the sharpness of the layer are established by the parameter $\beta>0$. For large β, the value of the third factor of (4.83) almost vanishes everywhere except in the vicinity of the internal layer. In the whole computation, the center is set as $(a,b)=(-0.01,-0.01)$ and the radius as $r_0=0.6$. We use the material properties of $(\lambda,\mu)=(2,1)$ and $\beta=1.0E+4$ while the estimator parameter is $\eta_\alpha=\eta_{0.5}$. The adaptivity gain in this Neumann problem is not as much as in the former punctual accumulation. Anyway, we still perceive the advantage of the adaptivity for all three polynomial degrees as shown by the results of the computation displayed in Fig. 3. Concerning the uniform case, one needs 73732, 294916, 663556 DOF to obtain the accuracies of $1.547191E+00$, $2.345337E-01$ and $2.926865E-02$ for $p=1,2,3$ respectively. As for the adaptive refinement, one needs 13864, 27404, 88132 DOF to achieve the accuracies of $6.941306E-01$, $9.318471E-02$ and $4.668647E-03$ respectively. By using the same order of DOF$\approx$ 200000, the precisions of $1.743901E-01$ (DOF=199916), $1.178998E-02$ (DOF=195944), $1.242509E-03$ (DOF=215080) are

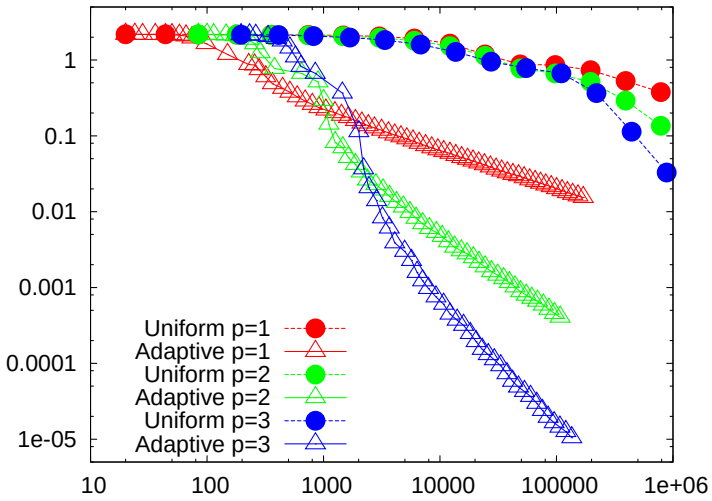

FIGURE 5. $\mathbf{H}^1$-accuracy in function of DOF by using the elastic properties $(\lambda, \mu) = (3, 2.5)$. Comparison of uniform and adaptive refinements for $p = 1, 2, 3$ for re-entrant corner.

obtained in the adaptive refinements for $p = 1, 2, 3$ respectively. We show in Fig. 4 four selected meshes from the adaptivity development where we use $p = 2$ and $\beta = 1.0E+4$. The displayed meshes contain respectively 18, 456, 2642 and 18994 elements. It is observed that the internal layer is automatically captured as the meshes become denser.

In this third test we perform a simulation in a domain admitting a re-entrant corner of internal angle 1.5π:

$$\mathbf{\Omega} = \big\{(-1,1)\times(-1,1)\big\} \setminus \big\{[0,1]\times[-1,0]\big\}. \tag{4.86}$$

The exact solution in both coordinates is

$$(x^2-1)(y^2-1)\exp\big[-\beta(x^2+y^2)\big]. \tag{4.87}$$

This function behaves very much like the exact solution of the punctual accumulation except that we do not have now a completely homogeneous Dirichlet boundary condition. The Neumann boundary corresponds to $\mathbf{\Gamma}_N = \big(\{0\}\times[-1,0]\big) \cup \big([0,1]\times\{0\}\big)$ while the Dirichlet boundary $\mathbf{\Gamma}_D$ to the remaining boundary part. We utilize the material properties $(\lambda, \mu) = (3.0, 2.5)$ while the a-posteriori estimator is $\eta_\alpha = \eta_{0.75}$ and the parameter $\beta = 1.0E + 04$. Although we have a re-entrant corner, the above exact solution is entirely smooth in $\mathbf{\Omega}$. Indeed, its higher derivatives are well defined everywhere although they have large smoothness bounds depending on β. For both the adaptive and the uniform refinements, the corresponding results for the polynomial degrees $p = 1, 2, 3$ are displayed in Fig. 5. In the case $p = 1$, the uniform refinement needs 785412 DOF to obtain the accuracy of $3.771127E-01$. In contrast, the adaptive

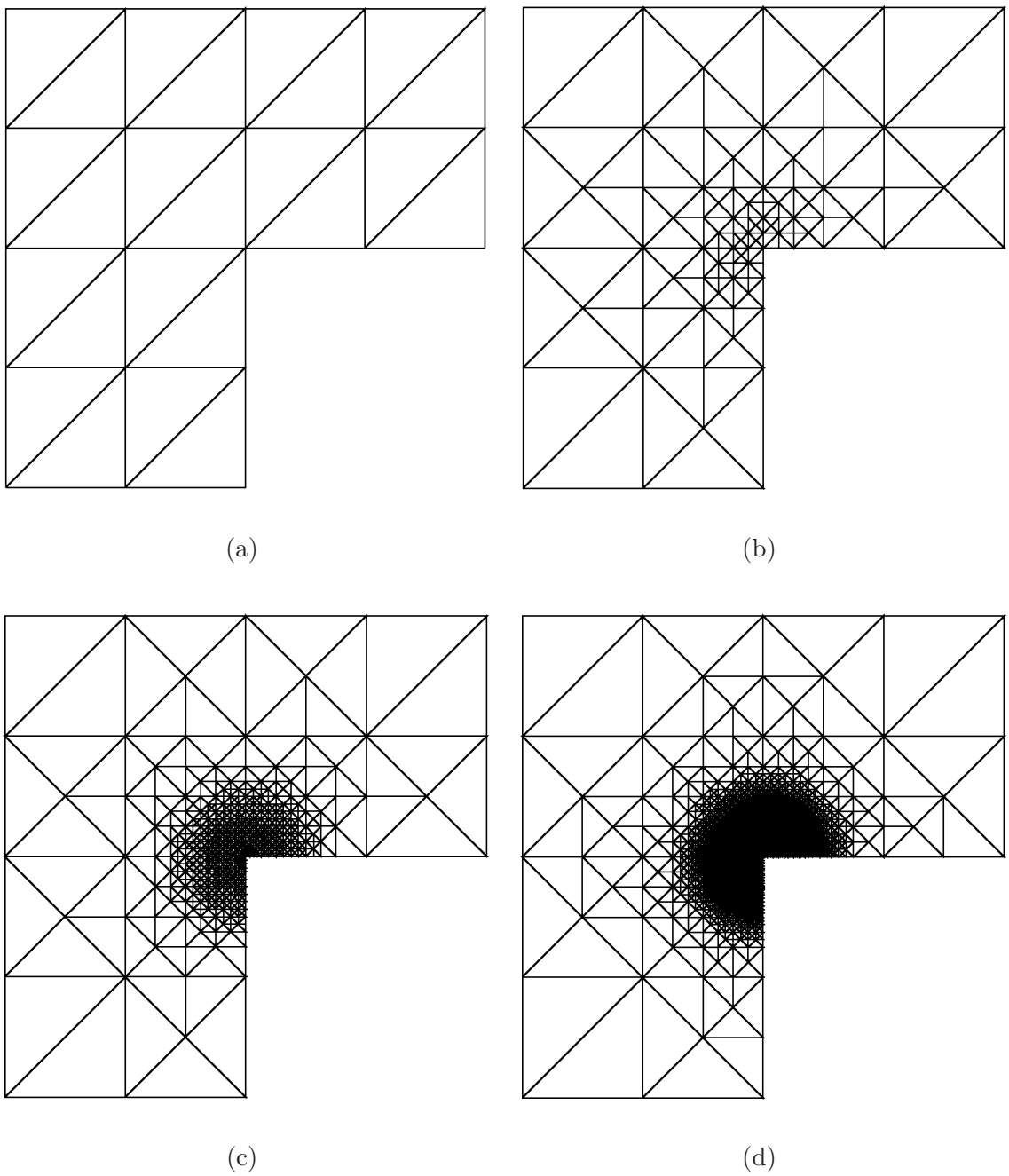

FIGURE 6. Refinement history for Neumann with a re-entrant corner where $p = 3$ and $\eta_\alpha = \eta_{0.75}$, $(\lambda, \mu) = (3.75, 1.25)$

refinement requires only 169748 DOF for the accuracy of $1.538906E-02$. As for $p = 2$, the uniform simulation necessitates 785412 DOF for the accuracy of $1.355110E-01$ while 107580 DOF yield the precision of $4.059962E-04$ in the adaptive case. Concerning $p = 3$, the uniform refinement needs 883204 DOF for $3.278068E-02$ while

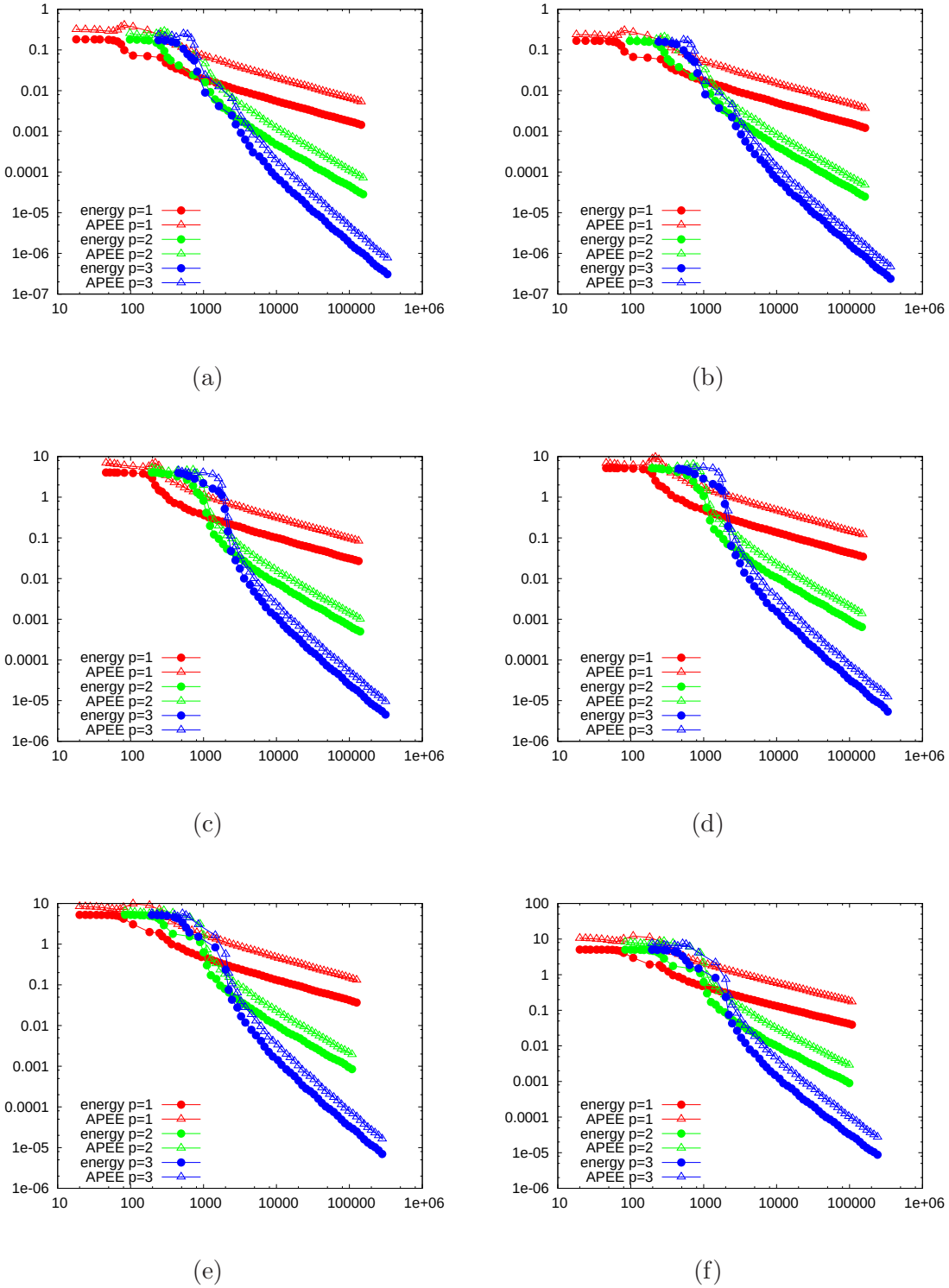

FIGURE 7. Comparison of energy precisions and the a-posteriori error estimates (APEE): (a)punctual accumulation for $(\lambda, \mu) = (1.85, 2.25)$, (b)punctual accumulation for $(\lambda, \mu) = (2.65, 1.55)$, (c)internal layer for $(\lambda, \mu) = (2.45, 1.25)$, (d)internal layer for $(\lambda, \mu) = (1.5, 3)$, (e)re-entrant corner for $(\lambda, \mu) = (3, 2.5)$, (f)re-entrant corner for $(\lambda, \mu) = (1, 3)$.

only 75844 DOF are needed for $2.377561E-05$ in the adaptive case. Thus, it turns out that similarly to the punctual accumulation, this Neumann simulation presents an advantage of the adaptive refinement over the uniform one for all three polynomial degrees. In addition, we consider different polynomial degrees having a similar DOF$\approx$ 100000. A precision of $2.010455E-02$ (DOF=100202) is obtained for the case $p=1$. For $p=2$, we have a precision of $4.059962E-04$ (DOF=107580) whereas a precision of $1.440417E-05$ (DOF=106984) is produced by $p=3$. Some selected adaptive refinement developments are displayed in Fig. 6 where the number of elements are respectively 24, 154, 1192 and 7346. The polynomial degree $p=3$ while the material properties correspond to $(\lambda,\mu)=(3.75,1.25)$, the sharpness parameter is $\beta=100$ and the a-posteriori error estimator is $\eta_\alpha=\eta_{0.75}$. It shows that the density of the mesh is very high in the neighborhood of the re-entrant corner.

The function of an APEE is not only to conduct an adaptive refinement, but also to supply an estimate of the precision of the computed FEM-solution. Therefore, we want now to compare the exact precision with the a-posteriori error estimates η_α. We consider the error in the energy norm (2.7) which depends on the material properties (λ,μ). The results are shown in Fig. 7 where we use the polynomial degrees $p=1,2,3$ for the former set of three benchmarks. On the horizontal axes, we have the DOF whereas the vertical axes show the energy accuracies and the a-posteriori error estimates. For each benchmark, we consider two different material properties and we use different values of η_α. For the punctual accumulation, we use the the material properties $(\lambda,\mu)=(1.85,2.25)$ and the a-posteriori error estimator $\eta_\alpha=\eta_{0.85}$ in Fig. 7(a). The second simulation for punctual accumulation is depicted in Fig. 7(b) where we use $(\lambda,\mu)=(2.65,1.55)$ and $\eta_\alpha=\eta_{1.0}$. Concerning the internal layer, we use the material $(\lambda,\mu)=(2.45,1.25)$ and the estimator $\eta_\alpha=\eta_{0.9}$ in Fig. 7(c) while $(\lambda,\mu)=(1.5,3)$ and $\eta_\alpha=\eta_{1.0}$ are used in Fig. 7(d). As for the re-entrant corner, the material properties are $(\lambda,\mu)=(3,2.5)$ and $(\lambda,\mu)=(1,3)$ while the estimators are $\eta_\alpha=\eta_{1.0}$ and $\eta_\alpha=\eta_{0.75}$ respectively in Fig. 7(e) and Fig. 7(f). We observe that the proposed estimators capture the exact precision up to some constant factors. In fact, the decrease of the exact and the estimated precisions follow the same pace as the adaptive refinements develop. We intentionally use various values of η_α in order to observe the effect of the parameter α. For all values of α, the results in Fig. 7 highlight that the estimator η_α provides an efficient estimation of the exact precision as predicted theoretically. In fact, the estimations by η_α are somewhat influenced by the values of the chosen α. Nonetheless, the values of η_α are comparatively of the same order up to some constant scaling factors. It turns out that the estimator can be used for both purposes, on the one hand to conduct a reliable adaptive refinements, as well as to estimate the FEM-accuracies on the other hand.

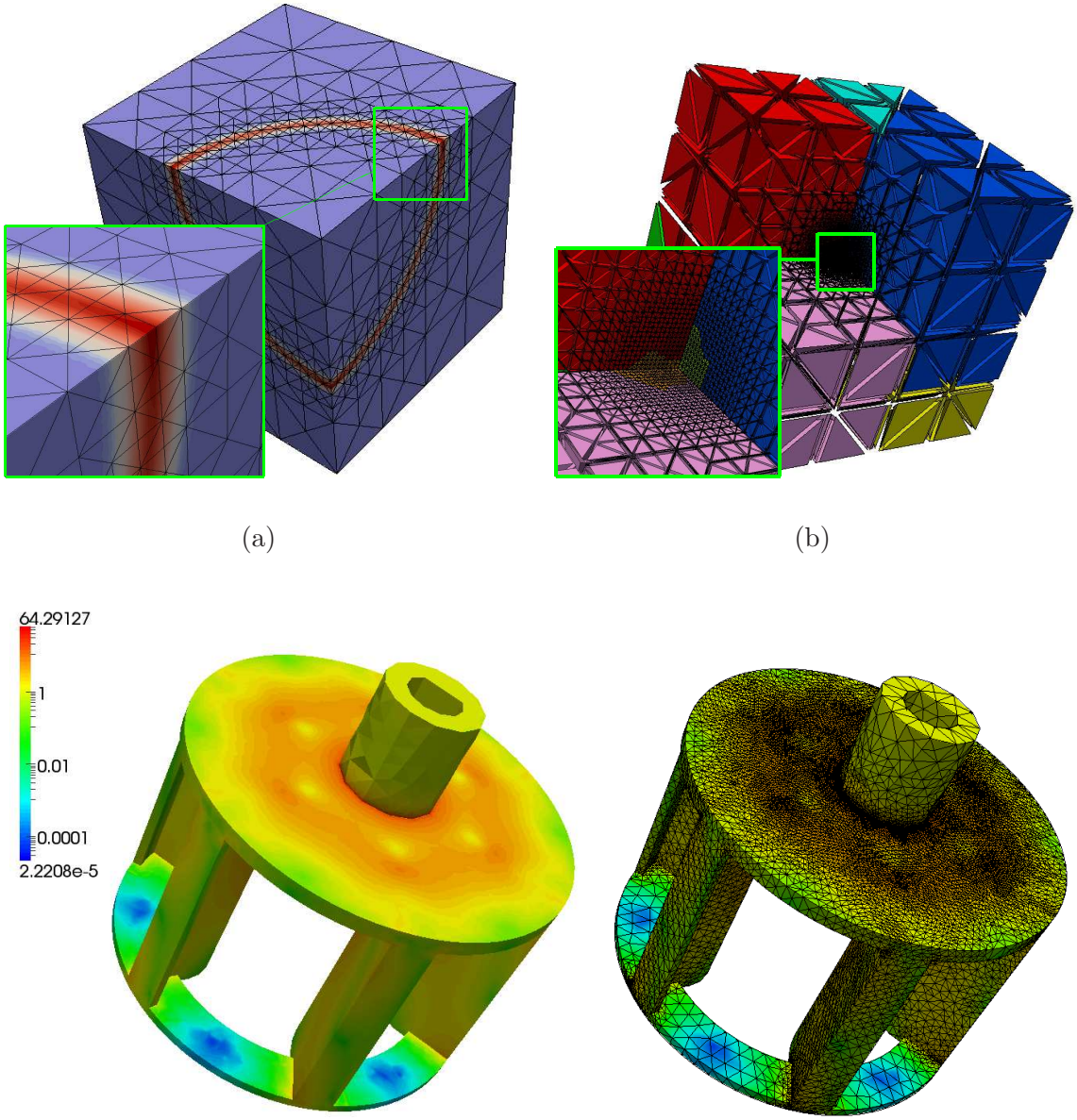

(a) (b)

(c) (d)

FIGURE 8. Some 3D results: (a)internal layer for $p = 3$, (b)adaptive and redistributed mesh on 8 processors for $p = 2$, (c)von Mises stress on a CAD model, (d)final mesh refinement.

The method has also been implemented in 3D which operates on parallel machines. We observe in Fig. 8(a) the 3D analogue of the previous internal layer. The result of an adaptive refinement where the mesh is distributed on 8 processors is depicted in Fig. 8(b). To achieve load balancing between the processors, the adaptive refinement

is combined with data redistribution. We have done a simulation on a realistic CAD model in Fig. 8(c) where the color map displays the von Mises stress in logarithmic scale. The final refinement is shown in Fig. 8(d) where the tetrahedral mesh tends to be dense at positions in which the von Mises stress is large.

Conclusion and future works

We investigated the use of a-posteriori estimator to conduct adaptive refinements for elastostatic simulations using a combination of Dirichlet and Neumann boundary conditions. It turns out that the estimator is reliable and efficient for assessing the FEM-accuracy. The estimator is valid for any polynomial degree which is constant in the entire mesh. Our numerical benchmarks include a punctual accumulation, an internal layer and a re-entrant corner. The a-posteriori estimates and the exact accuracy align well and the advantage of using higher polynomial degrees have been highlighted. The proposed approach works efficiently in the 3D-case using parallel implementations. We showed the advantage of using adaptive refinements controlled by the estimator over the uniform refinements. That significantly reduces the size of degrees of freedom without compromising on the accuracy.

Our future works in this direction might look as follows.

- For all the presented simulations with respect to elasticity, it turns out that using a higher polynomial degree coupled with adaptivity provides the best results. Its drawback in contrast to the piecewise linear setting is that it requires a denser stiffness matrix and a more sophisticated multilevel linear solver which will be presented in another document.
- For homogeneous materials, the dependence of the different constants on the Lamé parameters might be analyzed in the future. It is interesting to come up to an estimator where (λ, μ) appears. An extension to heterogeneous materials where the Lamé coefficients are variable in the domain is also interesting. The elastic stability is known to be very sensitive to those parameters as the materials approach compressibility.
- The previous point would necessitate a generalization of the Clément interpolant whose accuracy needs to be directly estimated in term of the elastic energy instead of the $\mathbf{H}^1$-norm. The construction of such an interpolant requires a polynomial lifting which extends a polynomial defined on an edge into an adjacent triangle in term of the elasticity energy norm.

References

[1] V. ADAMS, A. ASKENAZI, *Building better products with finite element analysis*, On-Word Press, 1999.

[2] M. AINSWORTH, T. ODEN, *A Posteriori error estimators for the Stokes and Oseen equations*, SIAM J. Numer. Anal. **34**, pp. 228–245, 1997.

[3] J. ALBERTY, C. CARTENSEN, S. FUNKEN, R. KLOSE, *Matlab implementation of the finite element method in elasticity*, Computing **69**, pp. 239-263, 2002.

[4] D. ARNOLD, A. MUKHERJEE, *Tetrahedral bisection and adaptive finite elements*, In: M. Bern, J. Flahery and M. Luskin, editors. Grid generation and adaptive algorithms (Minneapolis, MN, 1997), IMA Vol. Math. Appl. **113**, pp. 29–42. Springer, New York, 1999.

[5] D. ARNOLD, A. MUKHERJEE, L. POULY, *Locally adapted tetrahedral meshes using bisections*, SIAM J. Sci. Comp. **22**, No. 2, pp. 431–448, 1997.

[6] I. BABUSKA, M. SURI, *Locking effects in the finite element approximation of elasticity problems*, Numerische Mathematik **62**, No. 1, pp. 439–463, 1992.

[7] I. BABUSKA, M. SURI, *The hp-version of the finite element method with quasiuniform meshes*, ESAIM: Mathematical Modelling and Numerical Analysis **21**, No. 2, pp. 199–238, 1987.

[8] R. BANK, A. SHERMAN, A. WEISER *Some refinement algorithms and data structures for regular local mesh refinement*, In Scientific Computing, R. Stepleman et al. **44**, IMACS North-Holland, Amsterdam. pp. 3–17, 1983.

[9] C. BERNARDI, *Indicateurs d'erreur en h-N version des éléments spectraux*, Modélisation Mathématique et Analyse Numérique **30**, No. 1, pp. 1–38, 1996.

[10] C. BERNARDI, M. DAUGE, Y. MADAY, *Polynomials in the Sobolev world*, Preprint of the Laboratoire Jacques-Louis Lions, No. R03038, 2003.

[11] C. BERNARDI, Y. MADAY, *Polynomial interpolation results in Sobolev spaces*. Journal of Computational and Applied Mathematics **43**, No. 1–2, pp. 53–80, 1992.

[12] C. CARSTENSEN, S. BARTELS, *Each averaging technique yields reliable a-posteriori error control in FEM on unstructured grids. Part I: low order conforming, nonconforming, and mixed FEM*. Mathematics of Computation **71**, No. 239, pp. 945-969, 2002.

[13] C. DIEDRICH, D. DIJKSTRA, J. HAMAEKERS, B. HENNINGER, M. RANDRIANARIVONY, *A finite element study on the effect of curvature on the reinforcement of matrices by randomly distributed and curved nanotubes*, Journal of Computational and Theoretical Nanoscience **12**, pp. 2108–2116, 2015.

[14] M. DOBROWOLSKI, S. GRÄF, C. PFLAUM, *A Posteriori error estimators in the finite element method on anisotropic meshes*, ETNA **8**, pp. 36–45, 1999.

[15] Y. MADAY. *Analysis of spectral projectors in one-dimensional domains*, Mathematics of Computation **55**, No. 192, pp. 537–562, 1990.

[16] W. MCLEAN, *Strongly elliptic systems and boundary integral equations*, Cambridge University Press, Cambridge (2000).

[17] J. MELENK, B. WOHLMUTH, *On residual-based a posteriori error estimation in hp-FEM*, Adv. Comput. Math. **15**, No. 1–4, pp. 311-331, 2002.

[18] J. MELENK, *hp-interpolation of non-smooth functions*, SIAM J. Numer. Anal. **43**, pp. 127–155, 2005.

[19] M. RANDRIANARIVONY, G. BRUNNETT, *Preparation of CAD and molecular surfaces for meshfree solvers*, Lecture Notes in Computational Science and Engineering **65**, pp. 231–245, 2008.

[20] M. RANDRIANARIVONY, *FEM polynomial inverse estimates and elastostatic higher order estimator*, preprint 2018.

[21] M. RANDRIANARIVONY, *Harmonic variation of edge size in meshing CAD geometries from IGES format*. Lecture Notes in Computer Science **5102**, pp. 56–65, 2008.

[22] M. RANDRIANARIVONY, *Anisotropic finite elements for the Stokes problem: a-posteriori error estimator and adaptive mesh*, Journal of Computational and Applied Mathematics **169**, No. 2, pp. 255–275, 2004.

[23] M. RANDRIANARIVONY, *Geometric processing of CAD data and meshes as input of integral equation solvers*, Ph.D. thesis, Technical University of Chemnitz, Germany, 2006.

[24] M. RANDRIANARIVONY, *On global continuity of Coons mappings in patching CAD surfaces*, Comput.-Aided Design **41**, No. 11, pp. 782–791, 2009.

[25] M. RANDRIANARIVONY, *Stability of mixed finite element methods on anisotropic meshes*, Master's thesis, Faculty of mathematics, Technische Universität Chemnitz, 2001.

[26] K. SIEBERT, *An a posteriori error estimator for anisotropic refinement*, Numer. Math. **73**, No.3, pp. 373–398, 1996.

[27] M. SURI, *The p-version of the finite element method for elliptic equations of order* $2l$, Modélisation mathématique et analyse numérique **24**, No. 2, pp. 265–304, 1990.

[28] M. SURI, *The p and hp finite element method for problems on thin domains*, Journal of Computational and Applied Mathematics **128**, pp. 235-260, 2001.

[29] R. VERFÜRTH, *A-posteriori error estimation and adaptive mesh refinement techniques*, Journal of Computational and Applied Mathematics **50**, pp. 67–83, 1994.

[30] R. VERFÜRTH, *A-posteriori error estimators for the Stokes equations*, Numer. Math. **55**, pp. 309-325, 1989.

[31] M. VOGELIUS, *An analysis of the p-version of the finite element method for nearly incompressible materials. Uniformly valid, optimal error estimates*, Numerische Mathematik **41**, No. 1, pp. 39–53, 1983.

[32] B. WOHLMUTH, *A residual based error estimator for mortar finite element discretization*, Numer. Math. **84**, pp. 143–171, 1999.